7-31-2012

High pressure coolant effect on PVD coated inserts during end milling of Ti-6AL-4V

Arvind Sridharan

High pressure coolant effect on PVD coated inserts during end milling of Ti-6AL-4V

Date: 31st July 2012

A thesis submitted in partial fulfillment of the requirements for the Master of Science Degree in Industrial and Systems Engineering in Kate Gleason College of Engineering of Rochester Institute of Technology

Master of Science Candidate

Arvind Sridharan

Department of Industrial and Systems Engineering

Rochester Institute of Technology

Rochester, New York, USA

Committee Members

Andres L. Carrano
Associate Professor, Chair of Committee
Industrial and Systems Engineering
Kate Gleason College of Engineering

John L. Bonzo
Director, Brinkman Lab
Industrial and Systems Engineering
Kate Gleason College of Engineering

Brian K. Thorn
Associate Professor
Industrial and Systems Engineering
Kate Gleason College of Engineering

Denis R. Cormier
Earl W. Brinkman Professor
Industrial and Systems Engineering
Kate Gleason College of Engineering

ABSTRACT

Titanium alloys are being employed extensively in engineering and aerospace applications for their high strength to weight ratio, mechanical strength and ability to withstand high temperatures. Out of the different alloys of titanium available, the most commonly used alloy is Ti-6Al-4V. It is also called ‘Grade-5 titanium alloy’ or ‘α+β titanium alloy’. High speed machining of titanium alloys generates high temperatures in the cutting zone, promoting accelerated tool wear and reducing the efficiency in metal cutting. Consequently, the ability of the coolant to remove heat from the cutting zone plays an increasingly important role in the economics of the process as well as on the life of tool inserts. With the introduction of thru-tool coolant delivery, the coolant can now be delivered directly at the point of machining without having to flood the area of machining. This research tries to address the effects that high pressure and thru-tool coolant has on insert wear while end milling Ti-6Al-4V. The parameters used in this study are speed, feed, axial depth of cut, radial depth of cut and coolant pressure. A structured design of experiments along with a central composite design approach is used to determine the main effects of coolant pressure and its interactions with the remaining parameters. The results show that, within the parameters of this experiment, coolant pressure was not a significant main effect. However, pressure seems to react positively with feed rate. Contributions from this research can be used to recommend settings of the cutting factors in order to obtain the minimal tool wear.

KATE GLEASON COLLEGE OF ENGINEERING
ROCHESTER INSTITUTE OF TECHNOLOGY
ROCHESTER, NEW YORK

CERTIFICATE OF APPROVAL

MASTER OF SCIENCE DEGREE THESIS

The M.S. Degree Thesis of Arvind Sridharan
has been examined and approved by the thesis committee
as satisfactory for the thesis requirement for the
Master of Science degree

Andres L. Carrano, Ph.D. Advisor Chair of Committee	John L. Bonzo Committee Member
Brian K. Thorn, Ph.D. Committee member	Denis R. Cormier, Ph.D. Committee member

ACKNOWLEDGEMENT

It is my pleasure to thank everybody who has contributed to this thesis, and in some way or another made my time at the Industrial and Systems Engineering department at the Rochester Institute of Technology a great learning experience. I owe sincere and earnest thankfulness to all the faculty and staff of the ISE department who have contributed to the evolution and enrichment of this research.

I am truly indebted and thankful to my thesis advisor, Dr. Andres L. Carrano for his relentless support, thoughtful guidance, penetrating criticism and bountiful motivation. A special thanks to John L. Bonzo, who initiated this research and all through provided direction and support. Much of this work has been performed in the Brinkman Machine tools Lab, and John has been a tremendous help in procuring tools, machinery, equipment. Thanks to Dr. Brian Thorn for agreeing to be a part of the thesis committee and provide timely guidance. A special thanks to Dr. Denis Cormier, for his assistance with this research and the usability of the Hirox microscope.

I would like to show my gratitude to Mark Lawrence, Mike Standridge, Sean Holt and Karl Almquist from Sandvik Coromant, USA for the continued support with tools and guidance. Also a special thanks to ChipBlaster for loaning their High pressure coolant delivery system for this study. Last but not the least, I would like to express my sincere thanks to Scott Mincer from Morris Tri State, who trained and assisted me on the Okuma Multus B300. Current and former student assistants from the Brinkman Lab always lent their helping hand to troubleshoot problems.

It is never easy to travel half way around the globe, live away from your parents and siblings to study and earn a degree. I am obliged to my grandparents, parents and my brother who have stood unwaveringly by me through my education and without their encouragement this research would not have been complete. Thanks to my wife, Ridhi, for patiently being a part of this journey and sticking with me through the ups and downs of this project. Last, but not the least, thanks to Darla ‘Mom’ for the constant encouragement, reminder and support she has given me throughout my life at RIT.

Table of Contents Page

List of Figures

List of Tables

1. INTRODUCTION

Titanium alloys have unique inherent characteristics like high strength to weight ratio, temperature resistance, light weight, formability and corrosion resistance and hence are widely used in the aerospace, biomedical and chemical industries. However, titanium alloys are very difficult to work with due to high strength at high temperatures (Kahles, Field et al. 1985), low modulus, low thermal conductivity (Hong, Riga et al. 1993), and high chemical reactivity (Su, He et al. 2006). Ezugwu and Wang (1997) reported that about 80% of the heat generated in machining of titanium remains in the tool and only about 20% is carried away by the chip. Thus the tools used in machining titanium alloys are subjected to higher temperatures. Adding to this, the chips produced are thin and also the chip-tool contact length is very small. As a result the cutting stresses on the tool are very high and occur very close to the cutting edge of the tool. According to them, this leads to chatter mark on the workpiece surface and enhanced flank wear of the cutting tool.

Titanium and its alloys are classified as materials that are difficult to machine even at very low speeds (Komanduri and Von Turkovich 1981). The main problems in machining them are related to high cutting temperatures and rapid tool wear. The machining characteristics for titanium and its alloys are summarized by Hong, Markus et al. (2001)

- Titanium and its alloys are poor thermal conductors. As a result, the heat generated when machining titanium cannot dissipate quickly; rather, most of the heat is concentrated on the cutting edge and tool face.
- Titanium has a strong alloying tendency or chemical reactivity with the cutting tool material at tool operation temperatures. This causes galling, welding, and smearing, along with rapid wear or cutting tool failure.

- During machining, titanium alloys exhibit thermal plastic instability which leads to unique characteristics of chip formation. The shear strains in the chip are not uniform; rather, they are localized in a narrow band that forms serrated chips.
- The contact length between the chip and the tool is extremely short (less than one-third the contact length of steel with the same feed rate and depth of cut). This implies that the high cutting temperature and the high stress are simultaneously concentrated near the cutting edge (within 0.5 mm).
- Serrated chips create fluctuations in the cutting force; this situation is further promoted when alpha–beta alloys are machined. The vibrational force, together with the high temperature, exerts a micro-fatigue loading on the cutting tool, which is believed to be partially responsible for severe flank wear.

Ezugwu and Wang (1997) have effectively established that high cutting temperature acting close to the cutting edge during high speed machining of titanium alloys is the principle reason for rapid tool wear. Based on this, a reduction of tool wear while machining titanium alloys depends largely on the effectiveness of coolant/lubricant to dissipate heat from the cutting edge of the tool. However, it has been observed that limited work has been carried out in characterizing tool wear under varying coolant pressure conditions. This work aims to study the effects of coolant pressure on tool wear while end milling titanium alloy Ti-6Al-4V. The interaction of coolant pressure with other factors is also studied in this research.

1.1 Statement of problem

The motivation behind studying tool wear during end milling of Ti-6Al-4V, under different parameter conditions is to provide a better insight of the factors affecting the tool wear. By doing this, new cutting parameter zones, under high pressure coolant conditions, can be proposed in order to predict the nature of tool wear and also reduce the advent of tool wear. A quantitative characterization of the tool wear, taking into account the randomness of the wear pattern and interactive combinations of other factors is needed so that a robust process can be designed. This robustness will protect against the perturbations, both accountable and unaccountable, and help in gathering data and understand pressure as a main effect and its interaction with other parameters involved in the experiment. The design of experiment approach will consider the individual factors and the interactions while measuring the response. The objective of this research is to estimate the effect of pressure as a factor as well as its interacting factors and their effect on tool wear. Further, a region of optimum, in which the cutting conditions result in a lower tool wear, is sought through a response surface methodology.

2. LITERATURE REVIEW

2.1 Overview

The research related to machinability of titanium has been ongoing since the early 1970's. Most of the studies in the initial stages were focused on developing tools that could efficiently machine titanium and its alloys. In order to effectively and efficiently study the machining process of titanium, this literature review is split between machining of titanium alloy and high pressure coolant machining of alloyed materials.

2.1.1 Machining titanium alloys

Komanduri and Von Turkovich (1981) found that titanium and other aerospace structural super alloys are extremely difficult to machine except at low cutting speeds because of rapid tool wear. Their study was directed at chip formations while machining titanium. In end milling of the titanium alloy, high-speed machining up to a cutting speed of 628 m/min (20,000 rpm) is possible for sintered carbide tools. Measurements of cutting temperature during intermittent turning of a titanium disk, which is modeled on milling, reveal that the feasibility of high-speed end milling depends on a transient temperature rise or 'time-lag', owing to a short cut distance of the tool edge per single revolution, the existence of the helix angle, and a temperature drop through the use of a coolant (Kitagawa, Kubo et al. 1997). This temperature rise induces stress related wear and failures in the tool and hence the necessity of effective heat removal techniques from the cutting zone. High cutting temperature promotes thermally-related wear such as adhesion and diffusion. The fact that high cutting temperature acts so close to the cutting edge during high speed machining is the principle reason for tool wear (Ezugwu and Wang 1997). It therefore relates that tool life can be increased if the heat can be efficiently carried away from the cutting zone. This to a large extent depends on the effectiveness of the coolant provided to carry

away the heat from the cutting zone. Su, He et al. (2006) compared the tool life under dry cutting conditions versus directly injecting cooled nitrogen gas directly injected to the cutting zone. Figure 1 from the work mentioned, shows the plot of average flank wear against cutting time for various coolant conditions

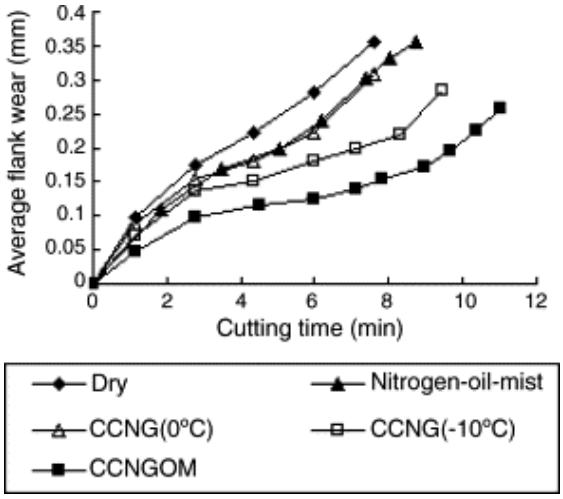

Figure 1: Average flank wear for various cooling/lubrication
(Source: Su, He et al. (2006))

In the plot, CCNG stands for Compressed Cooled Nitrogen Gas and CCNGOM stands for Compressed Cooled Nitrogen Gas and Oil Mist. Based on the experiment they drew several conclusions, one being "The dominant wear mechanism of coated cemented carbide tools was diffusion wear under all the cooling/lubrication conditions investigated except for flood coolant. Tool life was the shortest when using flood coolant due to severe thermal fatigue wear. Flood coolant seems not suitable for high-speed end milling of Ti-6Al-4V." Hong, Markus et al. (2001) argue that cryogenically cooling the workpiece is not desirable because the hardness of Ti-6Al-4V increases rapidly as the temperature is decreased. They compare pre-cooling the workpiece, indirect cooling, general flooding and an enclosed bath compared to the other approach of focused injection of liquid nitrogen into the cutting zone. The poor performance of conventional tools while machining of Ti-6Al-4V, fueled the need for newer cutting tools such as Cubic Boron

Nitride (CBN) and polycrystalline diamond to achieve high speed milling. However both CBN and polycrystalline diamond are very expensive and highly reactive to titanium. As a result Wang, Rahman et al. (2005) carried out an extensive study to investigate the wear patterns of BCBN (Bonded Cubic Boron Nitride) inserts used for high speed milling of Ti-6Al-4V. Their study consisted of comparing the CBN tools with BCBN tools under different cutting conditions. An average flank wear of 0.4 mm was considered as the tool failure criteria. In their study, López, Pérez et al. (2000) discuss the use of PVD coated tools in the milling of titanium alloys. They provide guidance to the values of the parameters that can be used while working with PVD coated tools and Ti-6Al-4V. The graph presented in Figure 2 shows the development of the flank wear vs. length of cut for two HSS mills, CrN and TiCN coated (V_c = 51 m/min), and for an uncoated hard metal mill (V_c = 100 m/min).

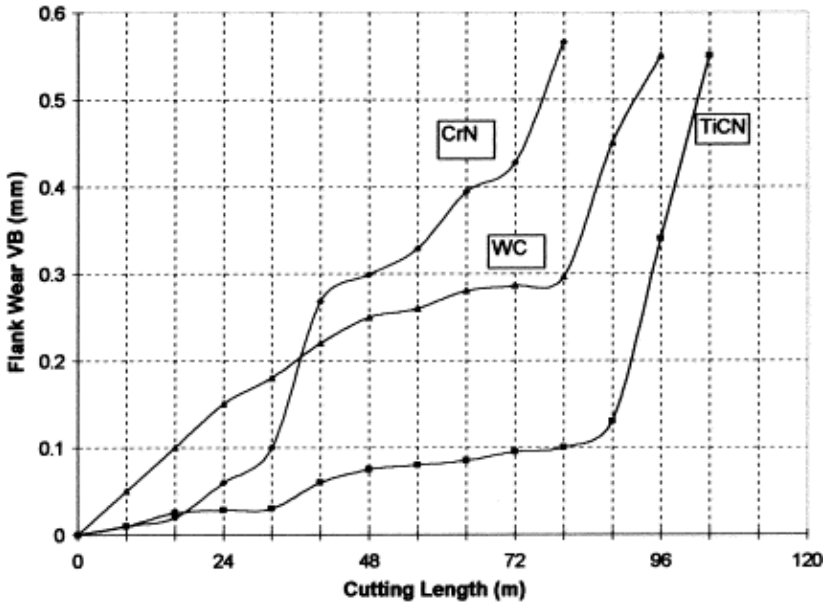

Figure 2: Development of flank wear in the machining of Ti–6Al–4V with both a coated (NCr and TiCN) and an uncoated hard metal tool
(Source: López, Pérez et al. (2000))

2.1.2 Machining with high pressure coolant

Wertheim, Rotberg et al. (1992) studied the phenomenon of "Influence of high-pressure flushing through the rake Face of the cutting tool". In this study it was found that flow rate and pressure have a significant influence on tool life and wear behavior as well as on the chip shape and the metallurgical structure of the chip itself. The narrowing and curling effect of the chip, improving chip exit from the slot, is viewed as related to temperature reduction. It was found that the phenomenon of built-up edge was minimized, especially when machining stainless steel and similar high alloy materials. Also tool life tends to improve with increasing coolant pressure. Ezugwu and Bonney (2004) also provided evidence that once a critical pressure has been reached, any further increase in coolant pressure may only result to a marginal increase in tool life In their paper "Effect of high-pressure coolant s upply when machining nickel-base, Inconel 718, alloy with coated carbide tools", Ezugwu and Bonney (2004), machined Inconel 718 with a triple PVD coated (TiCN/Al2O3/TiN) carbide tool at speeds up to $50\ \mathrm{m\ min^{-1}}$ using conventional and various high coolant pressures, up to 203 bar. The test results show that improved tool life can be achieved, under most cases, when machining Inconel 718 with high coolant pressures.

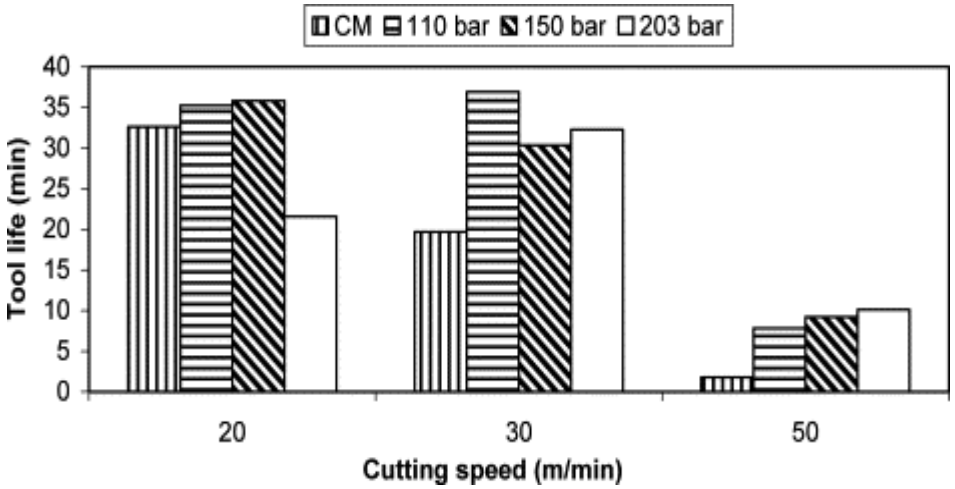

Figure 3: Tool life when machining Inconel 718 with various coolant pressures at a feed rate 0.25 mm/rev (CM: Conventional Machining)
(Source: Ezugwu and Bonney (2004))

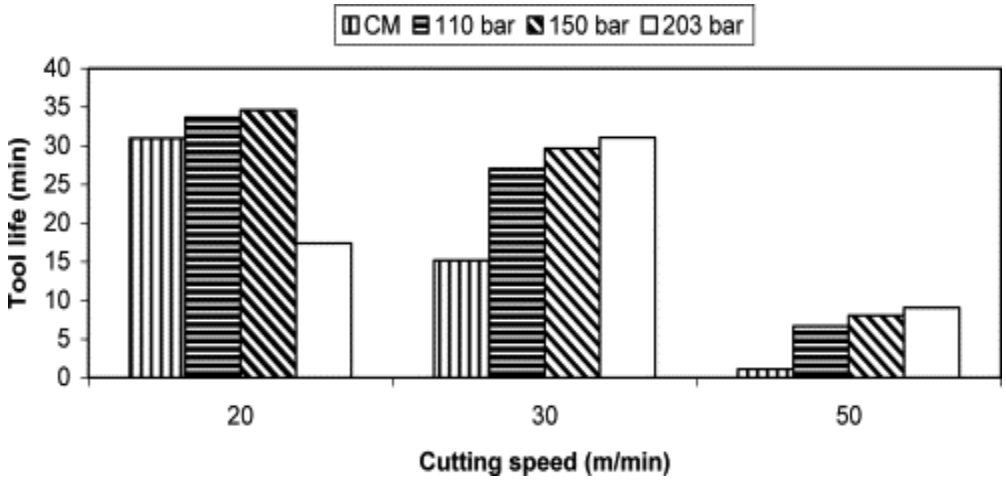

Figure 4: Tool life when machining Inconel 718 with various coolant pressures at a feed rate 0.3 mm/rev (CM: Conventional Machining)
(Source: Ezugwu and Bonney (2004))

Figure 3 and Figure 4, show that that, in most cases, longer tool life was achieved when machining with PVD coated carbide tool under high-pressure coolant supply than with conventional coolant supply. The authors conclude that coolants play a significant role in improving lubrication as well as minimizing temperature at the tool–chip and tool–workpiece interfaces, consequently, minimizing seizure during machining. Flood cooling does not seem to be effective in terms of lowering cutting temperature when machining exotic materials. Due to

high temperatures generated in the cutting zone, some of the coolant evaporates before it comes in contact with the chip-tool-workpiece interface.

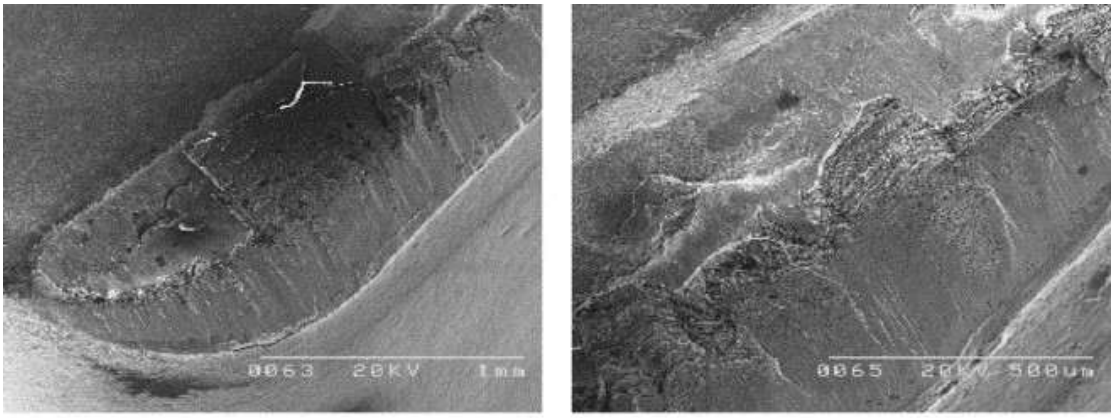

Figure 5:(a) Worn tool after machining Inconel 718 with 203 bar coolant pressure at a speed of 20 m/min and a feed rate of 0.3 mm/rev. (b) Enlarged view on the flank face showing abrasive wear and coating de-lamination of coated carbide tool
(Source: Ezugwu and Bonney (2004))

Figure 5 shows a typical worn tool illustrating nose-flank and rake-face wears. The uniform flank wear observed may be due to the low wear rate caused by temperature reduction at the cutting interface when machining with high coolant pressures. Ezugwu, Da Silva et al. (2005) evaluated the performance of CBN tools while turning Ti-6Al-4V under high pressure coolant conditions. Their paper evaluates the performance of different CBN tool grades in finish turning Ti–6Al–4V (IMI 318) alloy at high cutting conditions, up to 250 m min^{-1}, with various coolant supplies. Conventional coolant flow at 11 Mpa and 20.3 Mpa were conditions used in this experiment. Wear rate curves were plotted versus the cutting speeds, in Figure 6, for the different coolant pressures used in the experiment.

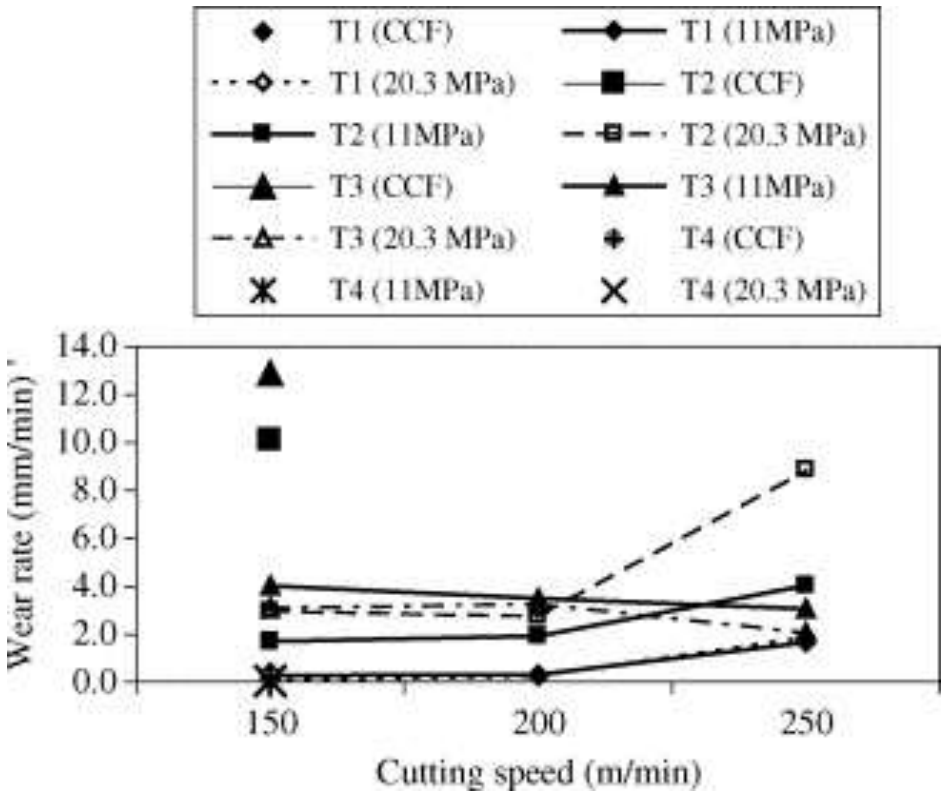

Figure 6: Wear rate curves when machining Ti–6Al–4V alloy with different CBN grade and uncoated carbide tools using conventional coolant flow and high pressure coolant
(Source: Ezugwu, Da Silva et al. (2005))

The authors conclude that conventional or low-pressure cooling methods fail to effectively conduct away the heat generated in the cutting zone, which is responsible for short tool life. Nandy, Gowrishankar et al. (2009) evaluated machining parameters such as chip form, chip breakability, cutting forces, coefficient of friction, contact length, tool life and surface finish of the finished workpiece by directing high-pressure coolant jets using neat oil and water-soluble oil. These results were compared to those done against conventional cooling methods. Figure 7 shows the photographic images of the tool wear comparisons.

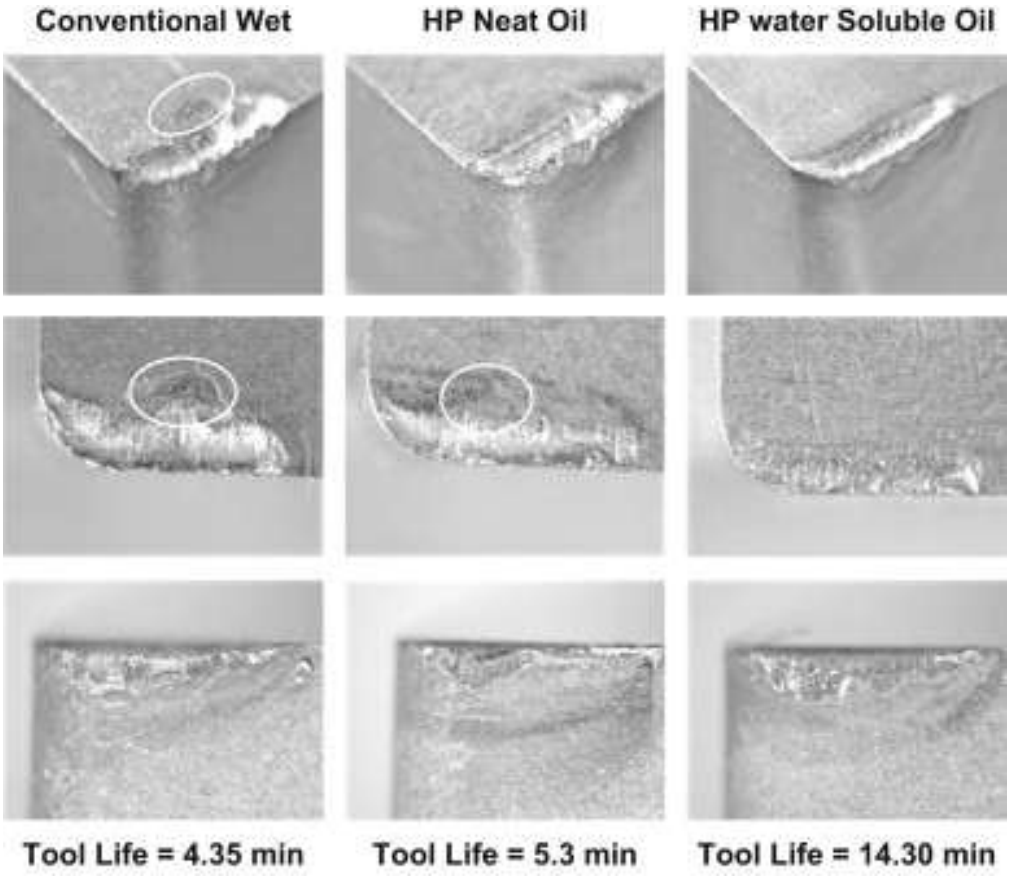

Figure 7: Worn cutting edges after turning of Ti–6Al–4V alloy at Speed=100 m/min, Feed=0.20 mm/rev, Pressure=100 bar and Nozzle dia.=0.8 mm under conventional wet, high-pressure neat oil and high-pressure water-soluble oil

(Source: Nandy, Gowrishankar et al. (2009))

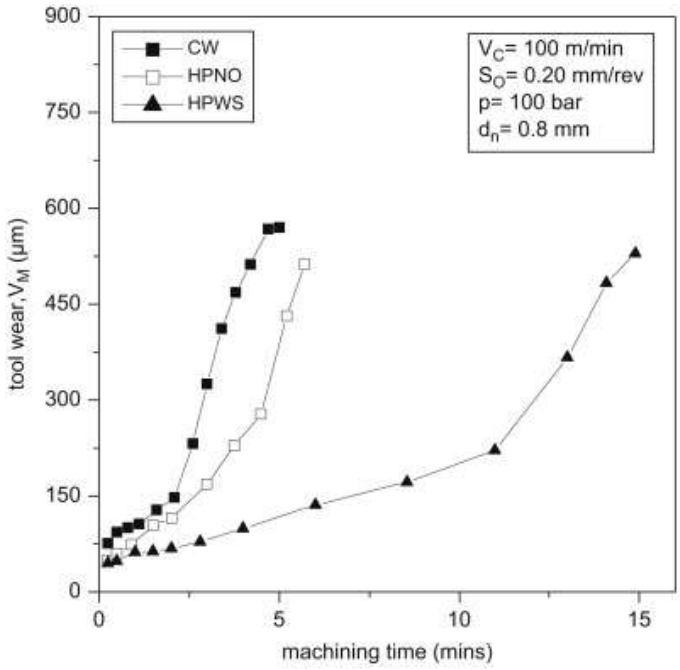

Figure 8: Growth of tool wear while turning Ti–6Al–4V alloy at *Speed*=100 m/min, *Feed*=0.20 mm/rev, *Pressure*=100 bar and *Nozzle Dia.*= 0.8 mm under conventional wet, high-pressure neat oil and high-pressure water-soluble oil
(Source: Nandy, Gowrishankar et al. (2009))

The growth curves of tool wear parameters shown in Figure 8 reveal steady initial rate of tool wear under conventional coolant, neat oil and water soluble oil coolants. According to the authors, typically higher tool wear sets in after reaching the maximum value of flank wear. The experiments were carried out using two-level half-factorial design with multiple central points. This enabled statistical analysis of data and developments of regression models between different machinability indices and machining and cooling parameters. Some of the conclusions drawn by Nandy, Gowrishankar et al. (2009) are: High-pressure cooling enables improvement in tool life and productivity by reducing the tool wear rate desirably. This is achieved by efficient cooling of the machining zone. High-pressure cooling also provided desirable chip breaking, which is essential in automated machining environment. Chip breaking has been more pronounced under

high-pressure water-soluble oil than high-pressure neat oil due to higher momentum of water-soluble oil and more chip curling owing to enhanced cooling under high-pressure water-soluble oil. In their paper on “High productivity rough turning of Ti-6Al-4V alloy, with flood and high-pressure cooling” Ezugwu, Bonney et al. (2009) investigated the performance of uncoated carbide tools when rough turning Ti-6Al-4V alloy under flood cooling and with 7 MPa coolant supply pressure. The dominant tool failure mode(s) were maximum flank and nose wear. Higher tool wear rates were observed when machining with flood cooling due to excessive temperature generation at the cutting interfaces, which accelerated tool wear.

3. MATERIALS AND METHODS

3.1 Overview

This chapter provides an overview of the materials, tooling, machines and statistical tools used in this experiment. Finally a brief introduction to the experimental methodology is discussed.

3.1.1 Materials

In this section the materials used for the experimentation are explained. It includes the work piece, tool, insert and coolant.

3.1.1.1 Work piece

The work piece used in this experiment is a 'α + β' alloy of titanium, also called Grade-5 titanium. The common name is Ti-6Al-4V which is derived from its chemical composition. Table 1 shows the nominal chemical composition of grade-5 titanium.

Table 1: Nominal chemical composition of Ti-6Al-4V

Material	**Percentage composition**
Al	5.5 – 6.76 %
V	3.5 – 4.5 %
C	< 0.08 %
Fe	< 0.25 %
N_2	< 0.05 %
O_2	< 0.2 %
H_2	< 0.01 %
Ti	Balance

Titanium alloys possess unique inherent characteristics, such as high strength to weight ratio, temperature resistance, low thermal conductivity, low modulus and high chemical resistivity. Some of the mechanical and physical properties of grade-5 titanium are showcased in Table 2 and Table 3

Table 2: Nominal mechanical properties of Ti-6Al-4V

Properties	**Typical Values**
Tensile Strength	1000 MPa
Elastic Modulus	910 GPa
Hardness Rockwell C	114

Table 3: Nominal physical properties of Ti-6Al-4V

Properties	**Typical Values**
Density	4.42 g/cm3
Melting Range	1649°C (±15°C)
Specific Heat	560 J/kg °C

The specimen for this experiment was engineered from a 5in. X 5in. X 4in. block. This block was cut using a band saw into a piece of dimension 2.5in. X 2.5in X 4in. used for all the experiments. Further, one end of the block was rounded on a lathe in order to for the block to be held in the 3 jaw chuck of the machine. Figure 9 shows the image of the titanium specimen used in the experiments.

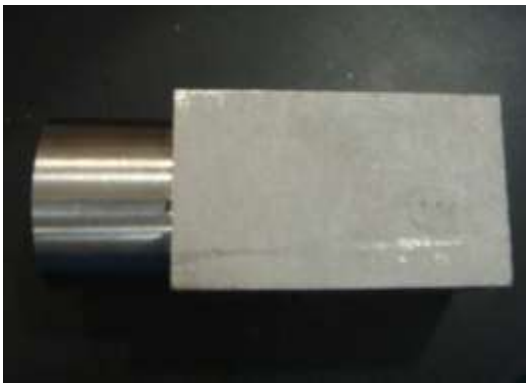

Figure 9: Titanium specimen

3.1.1.2 Tool

The tool used in this experiment was designed and provided by Sandvik Coromant. The tool is a CoroMill® 690 cutter and has a diameter of 44 mm. It is coupled with an adapter for use in the milling machine and the effective length for the tool is 160 mm. The tool has been specifically designed for profile and end milling applications in the aerospace industry. Figure 10 shows an actual photographic image of the tool used for this research. The cutter body has thru coolant capacity. Nozzles are designed along the flute of the cutter body. The nozzle size is 0.6 mm ID. Only three rows of the coolant holes are fitted with nozzles. The rest of the coolant holes were plugged in this study since these inserts were not use as cutting inserts.

Figure 10: CoroMill® 690 tool w/adapter

Figure 11: CoroMill® 690 cutter
(Source: Sandvik Coromant)

3.1.1.3 Insert

A cemented carbide insert with a PVD coating of 3.5 micrometer thickness, was used for this experiment. The edge-line has a 25 micron edge-rounding to give it increased edge-line strength. The tool has the capacity to be loaded with 6 rows of inserts with 3 inserts in each row. For the purpose of this experiment, only the bottom row with 3 inserts is utilized. The grade of the insert used is GC1030, designed for end milling. The insert is rhombic in shape with 10 mm. side. The nose radius is 1.2 mm and there are two cutting edges per insert. Figure 12 shows an image of the actual insert used in the experiments.

Figure 12: Insert used for the experiment

There are two cutting edges on each peripheral inserts. The insert has positive rake angles and has three different rakes for efficient removal of chips from the cutting interface. The geometry of the insert is optimized for titanium edging. Figure 13 shows the insert geometry.

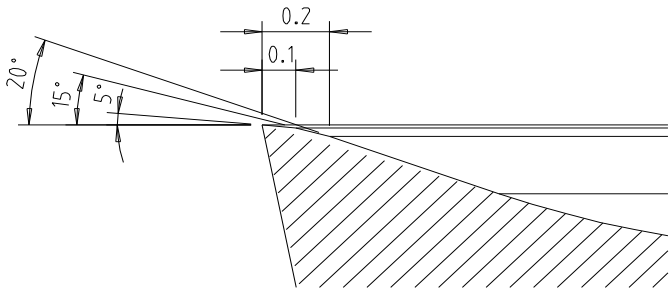

Figure 13: Insert geometry
(Source: Sandvik Coromant)

3.1.1.4 Coolant

An oil-water emulsion coolant is used for this experiment. Emulsion strength of 80% H_2O and 20% neat oil was maintained throughout the course of the experiment. BlassoCut, manufactured by Blaser Swiss lube, was the coolant used for this experimentation.

3.1.2 Machines

In this section, the primary machines used for the experimentation (cutting, coolant delivery and measurement of wear) are described.

3.1.2.1 Machining

An Okuma Multus B300, a 5-axis multifunctional machine was used for cutting the work piece. The machine has a 3 jaw chuck to hold the work piece. The Multus B300 has both multi-axis milling and turning capabilities. The rounded end of the specimen is held in the 3 jaw chuck and

using the CoroMill© 690 tool, the milling operation was performed. A machine level code language was written for the order of machining using the required parameters. Figure 14 shows the milling operation on the titanium specimen, using a CoroMill 690 cutter installed in the Okuma Multus B300. Detailed specification of the Multus B300 is provided in the appendix. For each experiment, three inserts were used in the bottom row. The machining operation performed was end milling. Length of cut for each milling operation was 9 mm. The desired parameters were entered into the CNC program code for each of the respective factors in the experiments and the program was run. After the desired experimental run was performed, the inserts were recorded, numbered and stored for measurement of wear. The surface of the specimen was cleaned and leveled by performing a series of face milling operations. This ensured that the conditions for all the experiments were identical.

Figure 14: Milling titanium using Multus B300

3.1.2.2 Coolant delivery

The ChipBlaster JV10 was used to deliver high pressure coolant for this experiment. The ChipBlaster high pressure coolant delivery system was interfaced with the Multus B300, for communication and controlling the parameters. The tool and the pressure of the coolant flowing through the tool were controlled using the Human - Machine Interface (HMI) on the Okuma Multus B300. The JV10 model had the capacity to vary the pressure from 200 psi to 1000 psi. The high pressure coolant pump also had the capacity to vary the coolant volume to maintain the desired coolant pressure. Figure 15 shows the ChipBlaster JV10 unit with the high pressure pump. Detailed specification of the JV10 is provided in the appendix section.

Figure 15: ChipBlaster JV10 HP coolant delivery

3.1.3 Wear measurement

A high resolution Hirox microscope was used to capture and measure the tool wear. The Hirox microscope has a linear XY stage base and an 85 mm travel range. It has a 35 – 2500x zoom capacity with a built in internal light source. It has a high resolution digital camera unit and comes with an inbuilt Hirox calibrated scale that automatically adjusts the scale when magnification ratio is changed. A fixture to locate the insert in order to measure the flank wear on the nose of the insert was printed using a Dimension Elite 3D printer. Figure 16 shows the insert positioned in the nest for wear measurement. Specifications of the Hirox microscope and Dimension Elite 3D printer are available in the appendix section.

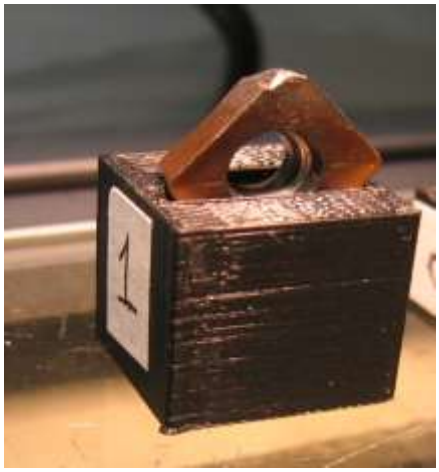

Figure 16: Locating fixture for insert

3.1.4 Procurement

There are very few instances in which an academic institution has been able to procure such expensive machines, tools and equipment to facilitate a graduate research. This would not be possible without the loans/donations made by the companies involved in this research and the dedication of the personnel at RIT to try and make this happen.

3.1.5 Statistical tools

In this section, the statistical tools used for this research have been briefly explained.

3.1.5.1 Fractional factorial experiment

A fractional factorial experiment is of the order $2^{(k-1)}$, where k stands for the number of factors in the experiment. In this form of an experiment, only a fraction of the complete experimental runs are performed. This experiment is most suitable in cases where time and cost determine the limitations on the number of experiments that can be performed. In a fractional factorial experiment, some of the main factors tend to be confounded with other factor interactions. In this case, the resolution of the design determines how the factors are confounded. For example, in a half fractional factorial design with 5 factors (A, B, C, D, E), the number of experimental runs will be $2^{(5-1)}$, i.e. 16 experimental runs. Further if the design generator, I=ABCDE, the main effects of all factors will be confounded with 4 factor interactions, ex. A + BCDE, and the 2 factor interactions were confounded with 3 factor interactions ex. AB + CDE, thus providing us information of all main effects and all 2 factor interactions.

3.1.5.2 Path of steepest ascent/descent

Direction of steepest descent is a gradient-based optimization technique. Experiments are executed in the direction of steepest descent, when the area of interest is minimization. Direction is found from the fitted equation. The experiments are iterated till the desired response is acquired. The procedure basically starts at the current operating conditions, then the linear model is fitted and the direction of steepest descent is determined. Experiments are iterated till no improvements are observed in the response. The direction of steepest descent is determined by the gradient of the fitted model and depends on the scaling convention. Usually the form of the

relationship between the response and the factors is unknown, so we find a lower order polynomial in this region that approximately explains this relationship. It may be a first order model or a second order model. Chances are that at the initial operating conditions X_1, $X_{2,}\ldots$, X_k are located far from the region of optimum. If the response is well modeled by a linear function of the independent variables, then the approximating function is the first order model is

$$y = \beta_0 + \beta_1 X_1 + \beta_2 X_2 + \beta_3 X_3 + \ldots\ldots\ldots + \beta_k X_k + \varepsilon$$

If there is curvature in the system, then the polynomial of a higher degree must be used, for example a second order model

$$y = \beta_0 + \sum_{i=1}^{k} \beta_i X_i + \sum_{i=1}^{k} \beta_{ii} X_i^2 + \sum_{i=1}^{k} \sum_{j=1}^{k} \beta_{ij} X_i X_j + \varepsilon$$

The procedure at this stage is to continue experimenting along the path of steepest descent until there is no further improvement in the response. Finding the step size in the direction of steepest descent is an important initial process step. It is a process of sequentially moving along the direction of minimization of the response. The coordinates of the factor settings in the direction of steepest descent separated by a distance ρ from the origin is given by

$$\text{Minimize } \beta_0 + \beta_1 X_1 + \beta_3 X_3 + \ldots\ldots + \beta_k$$

$$\text{Subject to } \sum_{i=1}^{k} X_i^2 \leq \rho^2$$

The direction of the gradient g, is given by the values of the parameter estimates, that is $g' = (\beta_1, \beta_2, \ldots\ldots, \beta_k)$

The coded factors x_i in the original units of measurement are obtained from the relation:

$$x_i = \frac{X_i - \frac{X_{low} - X_{high}}{2}}{X_{high} - \frac{X_{low}}{2}} \quad i = 1,2,3, \ldots, k$$

The solution is a simple equation which yields the coordinates. This coding convention is recommended since it provides parameter estimates that are scale independent, generally leading to a more reliable search direction.

$$x_i = \rho \frac{\beta_i}{\sqrt{\sum_{i=1}^{k} \beta_i^2}} \quad i = 1,2,3, \ldots \ldots, k$$

3.1.5.3 Central composite design

The motivation for a central composite design (CCD) comes from the sequential nature of the response surface methodology. The response surface methodology (RSM) is a collection of statistical and mathematical techniques useful for developing and optimizing the process. In most experiments, several input parameters influence the performance or quality characteristic of the process. This measure is called the response. The input variables are called the independent variables. The RSM is an analysis using graphical representation of the problem environment. In most cases the RSM is iterative and sequential in nature. Figure 17, shows the graphical representation of a response (on the y axis) for a given process with the process variables plotted on the x and z axes.

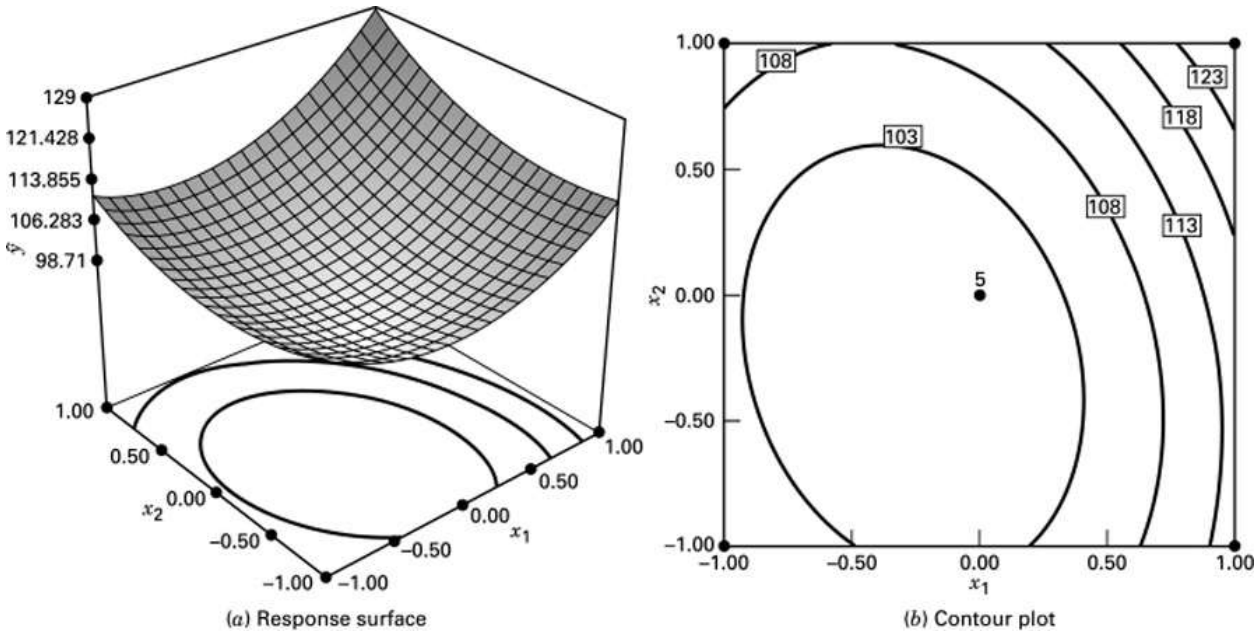

Figure 17: Response surface with contour plot
(Source: Design of Experiments – Douglas C. Montgomery)

3.1.6 Experimental overview

The objective of this research was to perform a series of experiments in order to estimate the impact of parameter values on the tool wear. Figure 18, shows the schematic representation of the factors that are the input to the experiment and tool wear as the output from the experimentation. The experiments were executed using Okuma Multus B300 and the ChipBlaster JV10 machines, located in the Brinkman machine tool laboratory at Rochester Institute of Technology. The wear measurement was done using a digital, high resolution Hirox microscope. The experiments were planned using statistical design of experiments and the run orders were completely randomized. Analysis of tool wear was performed using statistical tools provided by Minitab.

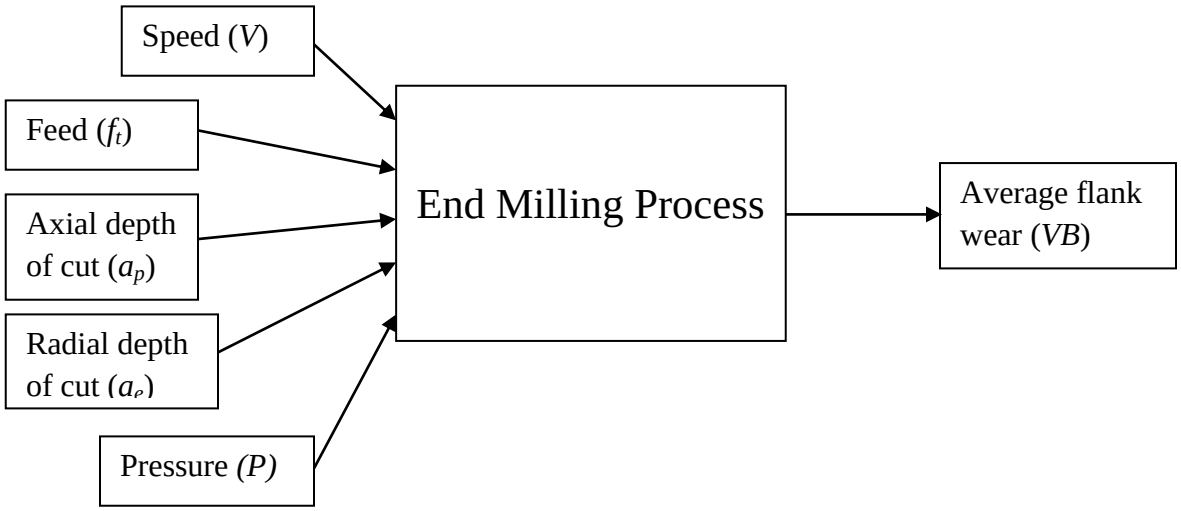

Figure 18: Schematic of parameters and response

3.1.6.1 Factors

Throughout the literature review, several authors (López, Pérez et al. (2000), Nouari and Ginting (2006), Jawaid, Sharif et al. (2000) have considered Speed, Feed, Axial depth of cut and Radial depth of cut as experimental factors. Based on these literature reviews and knowledge of the experiment the following five factors were considered for the experimentation process.

Speed (V) – Peripheral speed of the cutting tool measured at nominal diameter (m/min)

Feed (f_t) – Linear distance moved by the tool when one particular tooth is engaged (mm/tooth)

Axial Depth of Cut (a_p) – Distance that the tool is set below un-machined surface (mm)

Radial Depth of Cut (a_e) – Distance which the tool covers over the work piece surface (mm)

Pressure (P) – Coolant pressure pumped through the tool (psi)

3.1.6.2 Response

The output or response to be measured was insert wear. Maximum flank wear on the nose was the limiting factor that controlled tool life (Wang, Rahman et al. 2005). *Flank wear (VB)* is defined as loss of tool material from the tool flank as measured on the nose of the tool.

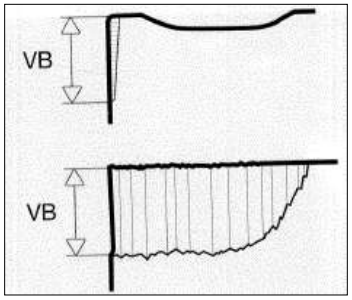

Figure 19: Flank wear
(Source: Handbook- Sandvik Coromant)

ISO 8688-2 describes the different forms of flank wear as:
Uniform Flank Wear (VB1) – Wear land which is normally of constant width
Non Uniform Flank Wear (VB2) – Wear land which has irregular width
Localized Flank Wear (VB3) – Exaggerated and localized to a specific part of the flank
A diagrammatic representation of the zones of flank wear has been shown in

Figure 20

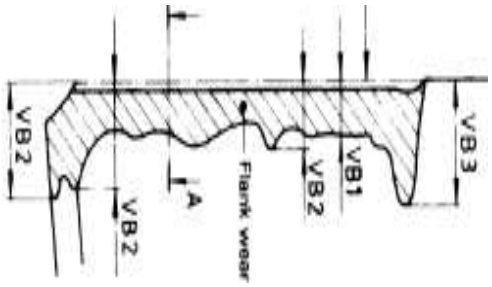

Figure 20: Flank wear zones
(Source: ISO 8688-2)

Using the guidelines set by ISO 8688-2, flank wear was measured on the nose flank of the insert. A reference line was set at the top of the insert. It is from this line that the uniform flank wear, localized flank wear and non-uniform flank wear were measured on the nose of the insert. The wear region that showed uniform wear pattern was judged and a line parallel to the reference line was drawn to mark this region. The perpendicular distance between these two lines was recorded as the uniform flank wear (VB1). Similarly parallel lines to the reference line were drawn at non uniform and localized flank wear points and the perpendicular distance from the reference line was calculated. Only the data for the uniform flank wear was recorded for this research. Three inserts performed the milling operation during each experimental run. Uniform flank wear (VB1) for each of these three inserts were measured and the average of the three readings were used as the uniform flank wear for the experimental run. Figure 21 shows an insert from the experimental run with uniform flank wear, non-uniform flank wear and localized flank wear.

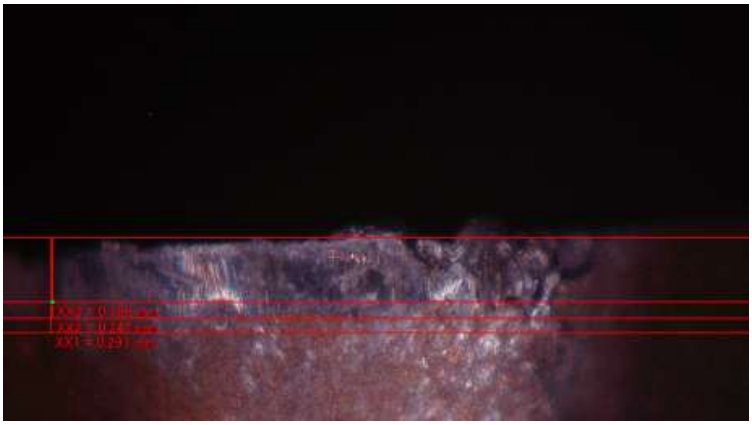

Figure 21: Insert showing VB1, VB2 and VB3

3.1.7 Experimental Methodology

Experimentation was done in 6 steps, following a systematic approach of designed set of experiments. Each step was followed by analysis and calculation for the next experiment.

Figure 22 explains the flow of the experimentation.

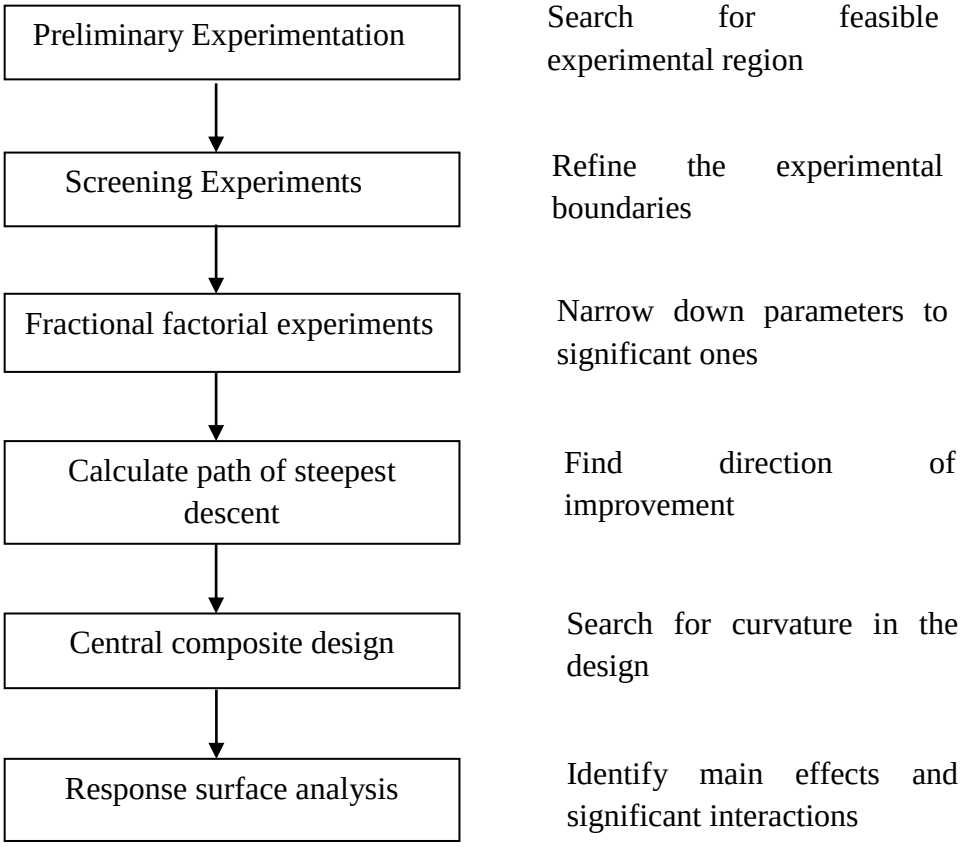

Figure 22: Experimentation flow diagram

4. EXPERIMENTATION AND RESULTS

Throughout the literature review several authors ((López, Pérez et al. 2000), (Nouari and Ginting 2006)), have considered Speed, Feed, Axial depth of cut and Radial depth of cut as factors for the experiments. Based on this information and knowledge of the experimentation, Speed (V), Feed (f_t), Axial Depth of cut (a_p), Radial Depth of cut (a_e) and Pressure (P) were the factors determined for this experimentation. Since the goal of this experiment was to study pressure both as a main factor and as an interacting factor with other parameters, no factor was eliminated during the process of experiments. The main effects of the parameters and the significance of interactions on the response were analyzed with a set of experimental runs. Only 2-factor interactions were considered significant and were studied. The response measured was average flank wear (VB), measured along the flank of the tool at the nose radius.

4.1 Preliminary experiments

The aim of this experimentation was to estimate the behavior of the insert at the lower level of the factor setting and compare it with the behavior at the higher end of the factor setting. The boundary parameters for this experiment (Table 4) were based on discussion with designers from a tool manufacturing company keeping in mind the suitable cutting conditions for the insert. The radial engagement, Radial depth of cut (a_e), was set at 13.2 mm for both the experimental runs.

Table 4: Factor levels – Preliminary experiments

Factor	Low Level (-)	High Level (+)
Speed (V)	30 m/min	60 m/min
Feed (f_t)	0.08 mm/tooth	0.1 mm/tooth
Axial depth of cut (a_p)	1.5 mm	2 mm
Pressure (P)	200 psi	500 psi

The factors for the first preliminary experiment were set at the high level, to estimate the interaction of the tool with the specimen. Table 5 shows the values set for the first preliminary experiment.

Table 5: First preliminary experiment

Factors	***Values***
Speed (V)	60 m/min
Feed (f_t)	0.1 mm/tooth
Axial DOC (a_p)	2 mm
Radial DOC (a_e)	13.2 mm
Pressure (P)	500 psi

The factors for the second preliminary experiment were set at the low level to estimate the interaction of the tool with the specimen. Table 6 shows the values set for the second preliminary experiment.

Table 6: Second preliminary experiment

Factors	***Values***
Speed (V)	30 m/min
Feed (f_t)	0.08 mm/tooth
Axial DOC (a_p)	1.5 mm
Radial DOC (a_e)	13.2 mm
Pressure (P)	200 psi

It can be seen in Figure 23 that the tool wear was beyond measurable capabilities for the preliminary set of experiments. Figure 23(a) shows the insert from the first preliminary experiment exhibiting catastrophic tool failure from excessive flank wear, while Figure 23(b) shows the excessive tool wear in the form of notching and build-up of material on the flank of

the insert for the second preliminary experiment. Since catastrophic tool failure was observed, further discussions about factor parameters were held with design experts from the tool manufacturing company.

(a) (b)

Figure 23: Insert wear - Preliminary experiment

4.2 Screening experiments

In order to refine the values of factors, further literature review was conducted. According to the literature, lower cutting speeds are preferred for titanium alloys (Komanduri and Von Turkovich 1981) and improvements are seen for cutting speeds of 55 m/min (Jawaid, Sharif et al. 2000). Also feed rates in the rage of 0.08 mm/tooth to 0.12 mm/tooth were found in the literature from López, Pérez et al. (2000) and Nouari and Ginting (2006). Based on these literature reviews, factor levels for screening experiment were refined. Table 7 shows the factors and their levels for the screening experiments.

Table 7: Factor levels – Screening experiment

Factor	Code	Low Level (-)	High Level (+)
Speed (V)	A	30 m/min	50 m/min
Feed (f_t)	B	0.05 mm/tooth	0.15 mm/tooth
Axial depth of cut (a_p)	C	1 mm	2 mm
Radial depth of cut (a_e)	D	13.2 mm	17.6 mm
Pressure (P)	E	200 psi	1000 psi

At this stage of experimentation, the objective was to gather additional information about the tool wear pattern and further study the factor levels. Also there was a limited quantity of titanium specimen available for this research. Considering this limitation and objective, a $2^{(5-1)}$ fractional factorial experiment with a resolution V design was the most suitable solution. The resolution V design ensured that none of the 2 factor interactions were compounded with the main factors.

Table 8: Response – Screening experiment

Run	A	B	C	D	E	Insert wear VB1 (mm)			Avg. VB1 (mm)
						1	2	3	
1	30	0.05	2	13.2	200	0.151	0.236	-	-
2	50	0.05	1	17.6	1000	-	0.259	-	-
3	30	0.15	2	13.2	1000	-	-	-	-
4	30	0.15	2	17.6	200	-	-	-	-
5	30	0.15	1	17.6	1000	0.757	-	-	-
6	50	0.15	2	17.6	1000	-	-	-	-
7	50	0.15	1	17.6	200	-	-	-	-
8	30	0.05	2	17.6	1000	0.410	-	0.327	-
9	30	0.05	1	13.2	1000	-	-	-	-
10	30	0.15	1	13.2	200	-	-	0.330	-
11	50	0.05	2	13.2	1000	-	0.497	-	-
12	50	0.15	2	13.2	200	-	-	-	-
13	30	0.05	1	17.6	200	0.252	-	-	-
14	50	0.05	1	13.2	200	-	-	-	-
15	50	0.15	1	13.2	1000	-	-	-	-
16	50	0.05	2	17.6	200	-	-	-	-

Again catastrophic failure was observed in the screening experiment. Data points marked with the sign '-' in Table 8 reflects that catastrophic failure was observed for several of the

experimental runs. Figure 24 shows images of inserts from the screening experiment. Figure 24(a) shows a broken insert from run #5 from the screening experiment. Figure 24(b) shows the insert from run #8 with excessive tool wear.

(a) (b)

Figure 24: Insert wear - Screening Experiment

Given the frequency of the occurrence of the insert failure, it was concluded that some factor levels needed readjustment. The fractional factorial experiment section describes the readjustment of the factor levels and the experiment conducted with the new factor levels.

4.3 Fractional factorial experiment

Since there was a limited quantity of titanium specimen available for experiments and three inserts were needed for each experimental run, fractional factorial of the order $2^{(5-1)}$ with a resolution V design was the most suitable design. The advantages of this design are that both main effects and 2 factor interactions remain un-confounded. Given the nature of the experiment and the cost involved for machining, this method of experiment provided the necessary information to take the experiment to the next level. Based on the results from the preliminary experiment, modifications were necessary for boundary conditions of some factors. In order to determine the factor levels for the fractional factorial, input from tool manufacturer was coupled with information from the literature. As the cutting speed increases, it exponentially increases

tool roughing, resulting in aggressive tool wear. López, Pérez et al. (2000), have similar findings in their paper. Given this information, the high level for cutting speed was reduced to 40 m/min. Jawaid, Sharif et al. (2000) have found improvements in tool performance for a feed rate of 0.1 mm/tooth. Also, as the radial depth of cut is increased, the chip thickness increases thereby increasing the temperature at the cutting edge. This high cutting temperature acting close to the cutting edge during high speed machining of titanium alloys is the principle reason for rapid tool wear (Ezugwu and Wang 1997). After discussion with the tool manufacturer, it was determined that the high level of the radial engagement be kept at 40% of tool diameter. Information about axial depth of cut was studied from literature ((Bajic, Lela, et al. 2008), (Nouari and Ginting 2006)) and set between 0.75 mm and 1.5 mm. Table 9 shows the factors and their levels for the fractional factorial experiment.

Table 9: Factor levels – Fractional factorial experiment

Factor	Code	Low Level (-)	High Level (+)
Speed (V)	A	30 m/min	40 m/min
Feed (f_t)	B	0.05 mm/tooth	0.10 mm/tooth
Axial depth of cut (a_p)	C	0.75 mm	1.5 mm
Radial depth of cut (a_e)	D	13.2 mm	17.6 mm
Pressure (P)	E	200 psi	1000 psi

The randomly generated design table for 16 runs of the experiment and the response is captured in Table 10. In this fractional factorial experiment, the design generator is E= ABCD. Therefore, the main effects were confounded with 4 factor interactions, ex. A + BCDE, and the 2 factor interactions were confounded with 3 factor interactions ex. AB + CDE.

Table 10: Response - Fractional factorial experiment

Run	A	B	C	D	E	Insert wear VB1 (mm)			Avg. VB1 (mm)
						1	2	3	
1	30	0.05	1.5	17.6	1000	0.223	0.295	0.248	0.255
2	30	0.05	1.5	13.2	200	0.306	0.250	0.254	0.270
3	40	0.1	0.75	17.6	200	0.437	0.206	0.189	0.277
4	40	0.05	1.5	13.2	1000	0.289	0.431	0.395	0.372
5	30	0.05	0.75	13.2	1000	0.196	0.229	0.121	0.182
6	40	0.05	0.75	13.2	200	0.227	0.322	0.225	0.258
7	30	0.05	0.75	17.6	200	0.158	0.273	0.293	0.241
8	40	0.1	1.5	13.2	200	1.306	1.421	1.319	1.349
9	40	0.1	1.5	17.6	1000	1.746	1.901	1.291	1.649
10	30	0.1	0.75	17.6	1000	0.214	0.221	0.179	0.205
11	40	0.1	0.75	13.2	1000	0.322	0.264	0.196	0.294
12	30	0.1	1.5	13.2	1000	0.668	0.686	0.703	0.686
13	40	0.05	1.5	17.6	200	0.589	0.535	0.412	0.512
14	30	0.1	1.5	17.6	200	0.691	0.587	0.543	0.607
15	30	0.1	0.75	13.2	200	0.297	0.295	0.281	0.291
16	40	0.05	0.75	17.6	1000	0.322	0.379	0.191	0.297

The fractional factorial experiment was intended to observe the trend in the response at various factor level combinations and evaluate the effect that the factors have on the response. Using this experiment and statistical analysis from the results, the idea was to model a response surface for further analysis to be conducted. Considering the scope of the research, all 3 factor interactions and higher were not analyzed. Figure 25 shows the different wear levels of inserts for the fractional factorial experiment. All images have the same magnification level of 100X and use the same light source and microscope settings. Figure 25(a) shows an insert from run #16 where

the average flank wear is 0.297 mm. Figure 25(b) shows an insert from run #11 where the average flank wear is 0.294 mm. Figure 25(c) shows an insert from run #7 where the average flank wear is 0.241 mm.

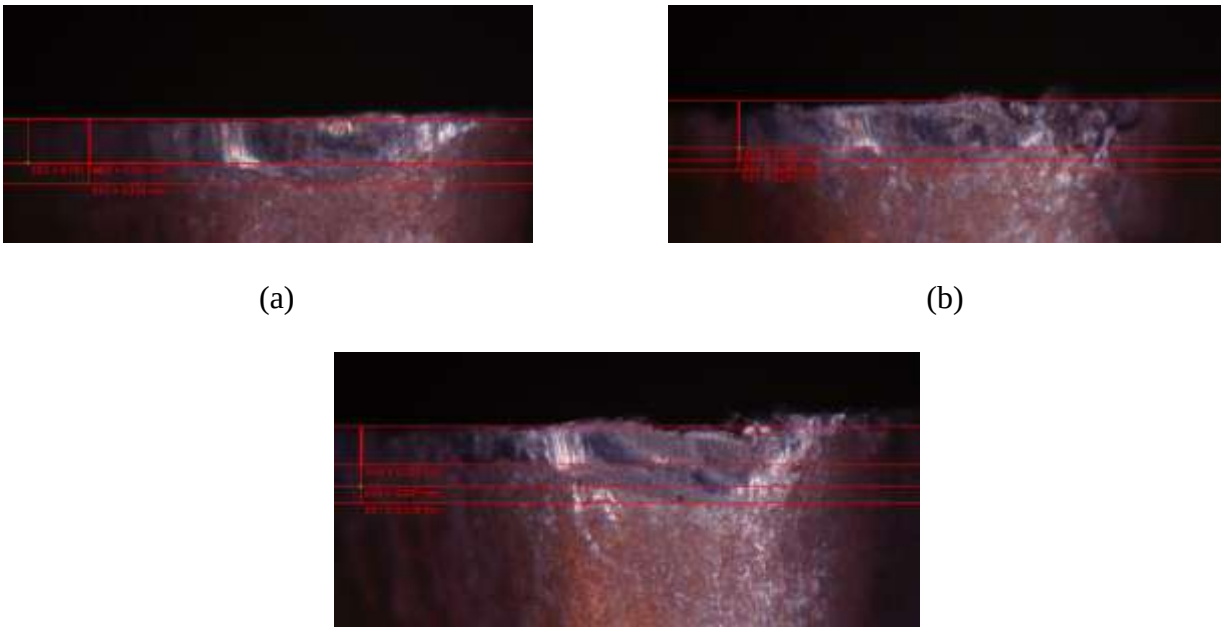

(a) (b)

(c)

Figure 25: Insert wear - Fractional factorial experiment

Regression analysis and analysis of variance was used to analyze the response. The analysis of data from this experiment will provide us with a suitable equation for the response surface. This surface can then be used to perform further analysis called response surface methodology to lead to a region of optimal solution.

The significance level considered throughout this experiment is 10%. Table 11 shows the p-values for all the main factors

Table 11: Analysis - Fractional factorial experiment

Predictor	Coefficient	Standard Error Coefficient	P value
Speed (V)	0.02839	0.01570	0.101
Feed (f_t)	7.428	3.140	0.040
Axial depth of cut (a_p)	0.6092	0.2093	0.016
Radial depth of cut (a_e)	0.00969	0.03568	0.792
Pressure (P)	0.0000211	0.0001962	0.917

The main effects plot is shown in Figure 26. All main effects have a positive slope, indicating that lower response is observed at lower levels of the factors.

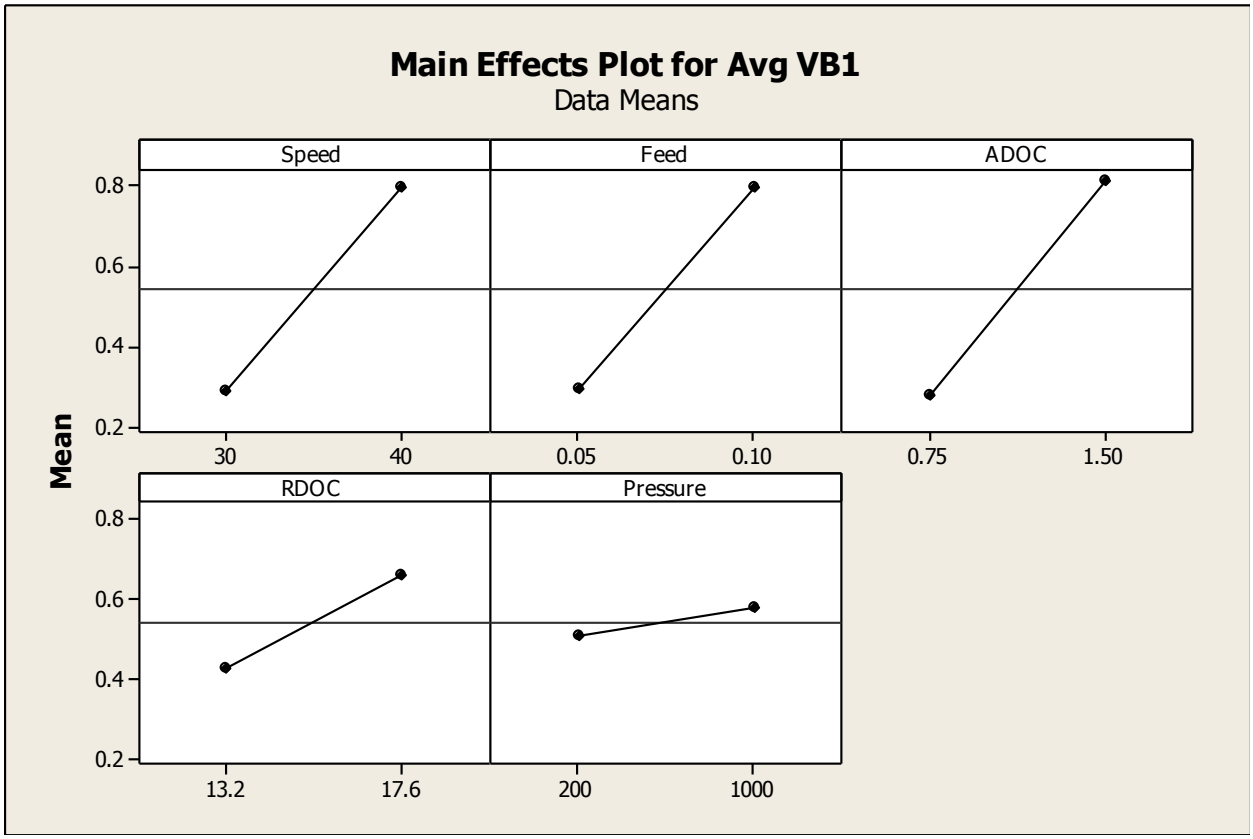

Figure 26: Main effects plot (data means) - Fractional factorial experiment

This means that observed insert wear is lower at the lower value of speed as compared to the higher value. Looking at the p-values, axial depth of cut (a_p), speed (V) and feed (f_t) have p-values less than or close to the significance level. P-value for pressure (P) is greater than 0.1 indicating that pressure (P) may not be a significant factor determining tool wear. Since no factors were intended to be dropped from the experiment, we analyze the equation of a first order model to fit the regression equation. Using statistical analysis, the response can be represented as an equation

Response (VB1) = -1.91 + 0.028 * Speed (V) + 7.43 * Feed (f_t) + 0.609 * Axial depth of cut (a_p) + 0.0097 * Radial depth of cut (a_e) + 0.000021 * Pressure (P)

The analysis of Variance in Table 12 below shows the diagnostic tests for the regression equation. This regression equation returns a p-value of 0.044 which is less than 0.1 showing conformance to the regression assumptions, although the R^2 values are not very high:

R^2 = 63.5%.

Table 12: Analysis of Variance – Regression equation

Source	DF	SS	MS	F	P
Regression	5	1.71736	0.34347	3.48	0.044
Residual Error	10	0.98592	0.9859		
Total	15	2.70328			

4.4 Path of steepest descent

Direction of steepest descent is a gradient-based optimization technique. Experiments are executed in the direction of steepest descent, when the area of interest is minimization. The direction is given by the fitted equation. The experiments are iterated until the desired response is reached. The procedure starts at the current operating conditions, and then the linear model is fitted and the direction of steepest descent is determined. Experiments are iterated until no improvements are observed in the response. The direction of steepest descent is determined by the gradient of the fitted model and depends on the scaling factor. The response is well modeled in the form of a first order regression equation of the form

$$y = \beta_0 + \beta_1 X_1 + \beta_2 X_2 + \beta_3 X_3 + \ldots\ldots\ldots + \beta_k X_k + \varepsilon$$

The direction of the gradient is given by the value of the parameter estimates, i.e. $\beta_1, \beta_2, \beta_3\ etc$. The coordinates of the factor settings in the direction of steepest descent are separated by a distance, ρ. This coding convention is used since it provides parameter estimates that are scale independent, generally leading to a more reliable search direction. x_i , then denoted the step size of each factor in the direction of improvement.

$$x_i = \rho \frac{\beta_i}{\sqrt{\sum_{i=1}^{k} \beta_i^2}} \qquad i = 1,2,3,\ldots\ldots,k$$

One can compute this equation for different increasing values of ρ and get different factor settings, all in the steepest descent direction. Since the co-efficient of feed has the largest absolute value, this is used to determine the step size. Using a coded value of

$\rho = 1$, $x_2 = 1$ then,

$$x_1 = \rho \frac{\beta_1}{\sqrt{\sum_{i=1}^{k} \beta_i^2}} = \frac{(1)(0.0284)}{\sqrt{(0.0284)^2 + (7.43)^2 + (0.609)^2 + (0.0097)^2 + (0.000021)^2}} = 0.0038$$

Similarly,

$$x_3 = \rho \frac{\beta_3}{\sqrt{\sum_{i=1}^{k} \beta_i^2}} = \frac{(1)(0.609)}{\sqrt{(0.0284)^2 + (7.43)^2 + (0.609)^2 + (0.0097)^2 + (0.000021)^2}} = 0.08$$

$$x_4 = \rho \frac{\beta_4}{\sqrt{\sum_{i=1}^{k} \beta_i^2}} = \frac{(1)(0.0097)}{\sqrt{(0.0284)^2 + (7.43)^2 + (0.609)^2 + (0.0097)^2 + (0.000021)^2}} = 0.0013$$

$$x_5 = \rho \frac{\beta_5}{\sqrt{\sum_{i=1}^{k} \beta_i^2}} = \frac{(1)(0.000021)}{\sqrt{(0.0284)^2 + (7.43)^2 + (0.609)^2 + (0.0097)^2 + (0.000021)^2}} = 0.0000028$$

From the above, to minimize the tool wear, the unit step size for each of the factors should be

Speed (V) = 5(0.0038) = 0.019 m/min

Feed (f_t) = 1(0.025) = 0.025 mm/tooth

Axial depth of cut (a_p) = 0.375(0.08) = 0.03 mm

Radial depth of cut (a_e) = 2.2(0.0013) = 0.0028 mm

Pressure (P) = 400(0.0000021) = 0.001 psi

The step sizes calculated for speed (V), feed (f_t), axial depth of cut (a_p), radial depth of cut (a_e) and pressure (P) are plugged into the regression equation obtained earlier to move along the direction of the descent till we reach the region of optimum. Once in this optimum zone, further experiments were conducted to check for curvature in the response surface. In Table 13, 'O' stands for the origin or the mid-point in the region of operability, while '▲' stands for the step size in the direction of improvement.

Table 13: Computing path of steepest descent

	Coded units					Uncoded units					VB1
	f_t	V	a_p	a_e	P	f_t	V	a_p	a_e	P	
O	0	0	0	0	0	0.075	35	1.125	15.4	600	
▲	1	0.0038	0.08	0.001	3 *10^-6	0.025	0.019	0.03	0.003	0.001	
O-▲	-1	-0.0038	-0.08	-0.001	-3 *10^-6	0.05	34.981	1.095	15.397	599.99	0.283
O-2▲	-2	-0.0076	-0.16	-0.002	-6*10^-6	0.025	34.962	1.065	15.394	599.99	0.079
O-3▲	-3	-0.0114	-0.24	-0.003	-9*10^-6	0.0	34.943	1.035	15.391	599.99	-0.125

Table 13 shows the value of the response changes from a positive value to a negative value at the 'O-3▲' level. This means that the vector changes direction in this region. Practically, this means that the factor levels at 'O-2▲' should produce the minimum flank wear. The corresponding values of the factors obtained from this region of optimum are found in Table 14.

Table 14: Factors at O-2▲

Factors	***Values***
Speed (*V*)	35 m/min
Feed (f_t)	0.025 mm/tooth
Axial DOC (a_p)	1.065 mm
Radial DOC (a_e)	15.4 mm
Pressure (*P*)	600 psi

4.5 Central composite design

The motivation for a central composite design (CCD) comes from the sequential nature of the response surface methodology. RSM (response surface methodology) is an analysis using graphical representation of the problem environment. A half fractional factorial design coupled with 4 center points and 10 axial points was designed. The factorial points represent a variance optimal design for the model. Center points are used to identify the curvature in the system. The set of axial runs allows for efficient estimation of pure quadratic terms. The center points provide an estimate of pure error and contribute to the estimation of the pure quadratic terms. The axial points are calculated based on an alpha (α) value. The values of the factors for this design come from the calculation of steepest descent. In order to keep the value of pressure at the axial points limited to 1000 psi (limitations imposed by the machine), the alpha value for this CCD design was set at α=2. Using the values of factors from the steepest descent calculation, factor levels for the CCD were set. Table 15 shows the factors and their levels for the experiment.

Table 15: Factor Levels – Central Composite Design

Factor	Code	Factor level at axial points	Factor level at cube points	Factor level at center point
Speed (V)	A	33 m/min 37 m/min	34 m/min 36 m/min	35 m/m
Feed (f_t)	B	0.015 mm/tooth 0.035 mm/tooth	0.020 mm/tooth 0.030 mm/tooth	0.025 mm/tooth
Axial depth of cut (a_p)	C	1.053 mm 1.093 mm	1.063 mm 1.083 mm	1.073 mm
Radial depth of cut (a_e)	D	14.6 mm 16.2 mm	15.0 mm 15.8 mm	15.4 mm
Pressure (P)	E	600 psi 1000 psi	700 psi 900 psi	800 psi

Table 16: Response - Central composite design

Run	A (Speed)	B (Feed)	C (ADOC)	D (RDOC)	E (Pressure)	Insert wear VB1 (mm)			Avg. VB1 (mm)
						1	2	3	
1	34	0.020	1.083	15.8	900	0.364	0.339	0.351	0.351
2	33	0.025	1.073	15.4	800	0.273	0.252	0.229	0.251
3	35	0.025	1.073	16.2	800	0.237	0.202	0.221	0.220
4	36	0.020	1.063	15.0	700	0.339	0.256	0.327	0.307
5	35	0.025	1.053	15.4	800	0.300	0.376	0.376	0.351
6	35	0.025	1.073	15.4	1000	0.227	0.270	0.285	0.261
7	36	0.030	1.063	15.0	900	0.285	0.360	0.324	0.323
8	34	0.030	1.063	15.8	900	0.256	0.220	0.231	0.236
9	35	0.025	1.073	15.4	800	0.164	0.391	0.439	0.331
10	34	0.020	1.063	15.8	700	0.187	0.221	0.191	0.200
11	34	0.020	1.083	15.0	700	0.306	0.308	0.333	0.316
12	35	0.025	1.073	15.4	800	0.343	0.356	0.339	0.346
13	36	0.030	1.063	15.8	700	0.258	0.383	0.381	0.341
14	34	0.030	1.083	15.8	700	0.324	0.320	0.302	0.315
15	36	0.030	1.083	15.0	700	0.322	0.368	0.354	0.348
16	36	0.020	1.063	15.8	900	0.250	0.333	0.324	0.302
17	35	0.015	1.073	15.4	800	0.289	0.320	0.279	0.296
18	36	0.020	1.083	15.0	900	0.331	0.352	0.320	0.334
19	35	0.025	1.073	14.6	800	0.337	0.349	0.308	0.331
20	35	0.025	1.093	15.4	800	0.187	0.387	0.352	0.309
21	35	0.025	1.073	15.4	800	0.310	0.360	0.326	0.332
22	35	0.025	1.073	15.4	800	0.221	0.424	0.349	0.331
23	36	0.030	1.083	15.8	900	0.225	0.378	0.362	0.322
24	34	0.030	1.063	15.0	700	0.293	0.337	0.297	0.309
25	35	0.035	1.073	15.4	800	0.297	0.337	0.327	0.320
26	34	0.020	1.063	15.0	900	0.304	0.327	0.329	0.320
27	35	0.025	1.073	15.4	600	0.314	0.376	0.343	0.344
28	37	0.025	1.073	15.4	800	0.333	0.295	0.322	0.317
29	34	0.030	1.083	15.0	900	0.225	0.401	0.372	0.373
30	36	0.020	1.083	15.8	700	0.285	0.366	0.337	0.329

Table 16 shows the sixteen runs conducted at cube points, ten runs done at axial points and four runs conducted at center points. The goal of this experiment was to establish the effects of pressure on the wear rate. Also in addition, the interaction of pressure with other factors was of particular interest.

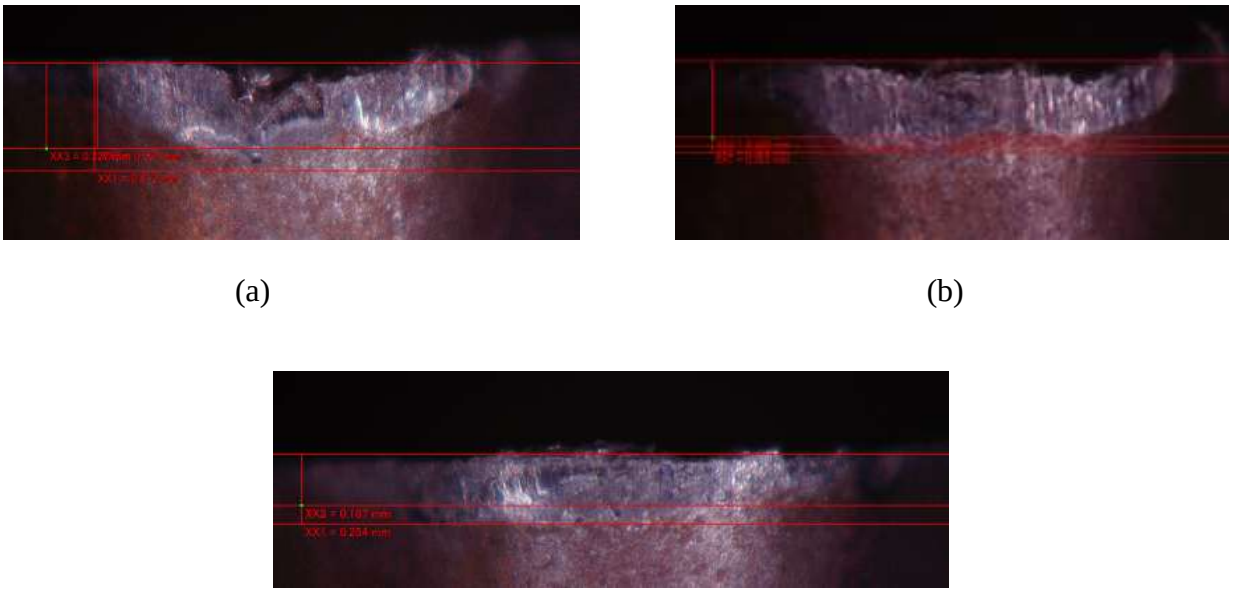

(a) (b)

(c)

Figure 27: Insert wear - Central composite design

Figure 27 shows the different wear levels of inserts for the central composite design. All images have the same magnification level of 100X and use the same light source and microscope settings. Figure 27(a) shows the insert wear from the run# 25 with a average flank wear of 0.320 mm. Figure 27(b) shows the insert wear from the run# 17 with a average flank wear of 0.296 mm. Figure 27(c) shows the insert wear from the run# 10 with a average flank wear of 0.200 mm. The objective of this experiment was to identify if pressure was a main factor influencing the wear rate and also to plot the response surface of interaction of other factors with pressure. Response surface regression and analysis of variance was used to study the response.

Table 17: Analysis – Central composite design

Predictor	Coefficient	Standard Error Coefficient	P value
Speed (V)	0.963	0.984	0.344
Feed (f_t)	127.187	205.654	0.546
Axial depth of cut (a_p)	5.035	45.499	0.913
Radial depth of cut (a_e)	-3.682	2.436	0.153
Pressure (P)	0.003	0.010	0.741
Pressure (P)* Speed (V)	-0.000	0.000	0.313
Pressure (P)* Feed (f_t)	-0.032	0.017	0.086
Pressure (P)* Axial depth of cut (a_p)	0.000	0.009	0.954
Pressure (P)* Radial depth of cut (a_e)	-0.000	0.000	0.977

Table 17 shows the p-values of the main effects and the interactions.

Table 18: Analysis of variance – Central composite design

Source	Seq. SS	Adj. SS	Adj. MS	F	P
Speed (V)	0.0053	0.0011	0.0011	0.96	0.344
Feed (f_t)	0.0005	0.0004	0.0004	0.38	0.546
Axial depth of cut (a_p)	0.0021	0.0000	0.0000	0.01	0.913
Radial depth of cut (a_e)	0.0072	0.0027	0.0027	2.29	0.153
Pressure (P)	0.0005	0.0001	0.0001	0.11	0.741
Pressure (P)* Speed (V)	0.0012	0.0012	0.0012	1.09	0.313
Pressure (P)* Feed (f_t)	0.0040	0.0040	0.0040	3.40	0.086
Pressure (P)* Axial depth of cut (a_p)	0.0000	0.0000	0.0000	0.0	0.954
Pressure (P)* Radial depth of cut (a_e)	0.0000	0.0000	0.0000	0.0	0.977

The p-values from the analysis of variance Table 18 for insert wear (VB) suggest a possible interaction between Pressure (P) and Feed (f_t). The analysis of variance returned an R^2 value of R^2 = 62.25%. To check the effect of interaction terms, contour plots for flank wear (VB) for

pressure versus interacting factors are plotted. This will help in understanding any curvature, if present, in the experiment.

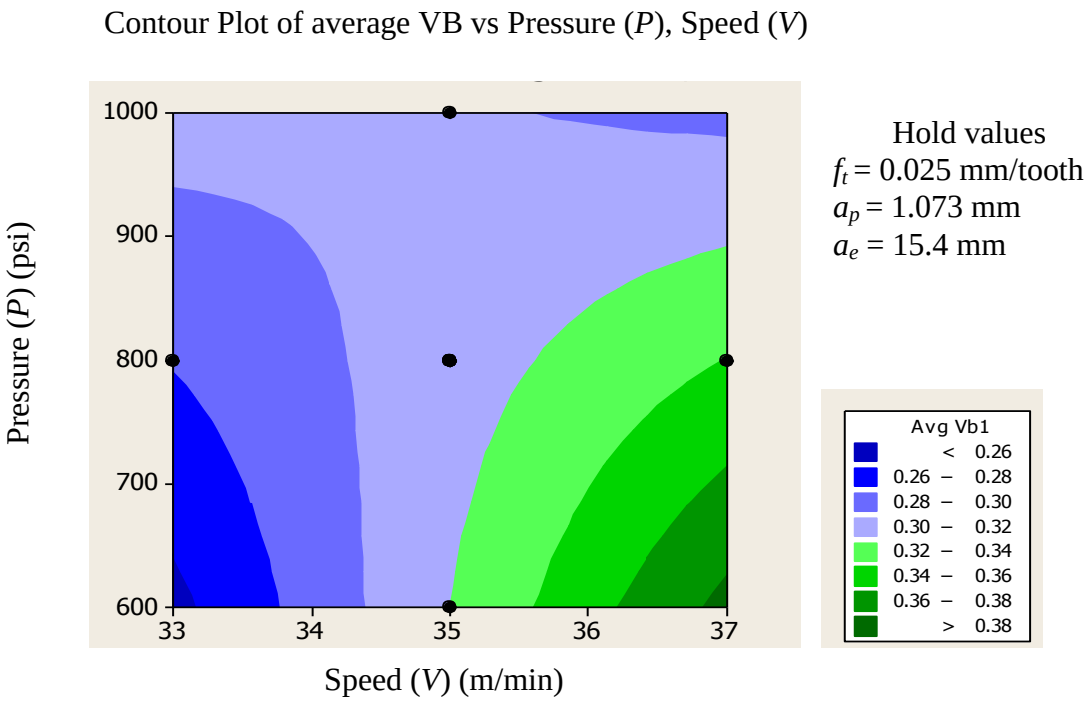

Figure 28: Contour plot (*P* vs. *V*)

Figure 28 shows the contour plot of Pressure (*P*) versus Speed (*V*), where curvature in the surface can be observed. At a pressure value of 600 psi, moving from the low speed setting to the high speed setting, insert wear continues to increase. One explanation for this increase in insert wear is the increase in tool roughing as cutting speed is increased. Moving from the low speed setting to the high speed setting at pressure value of 1000 psi, there is no increase in the insert wear. At the high speed and high pressure setting, a decrease in tool wear is observed. This could mean that beyond 1000 psi of coolant pressure, a decrease in tool wear may be observed. As the pressure increases, it effectively breaks the chips and removes the heat generated at the cutting tool interface. Nandy, Gowrishankar et al. (2009) have drawn conclusions that high pressure coolant effectively reduces the heat from the cutting zone during turning of Ti-6Al-4V. A

counter phenomenon of high pressure coolant is also abrupt or random breakages of chips. This causes tool roughing and an increase in tool wear may be observed. This could be one explanation for the increase in insert wear observed when the speed is kept constant at 33 m/min and pressure is increased from 600 psi to 1000 psi and an increase in insert wear is observed.

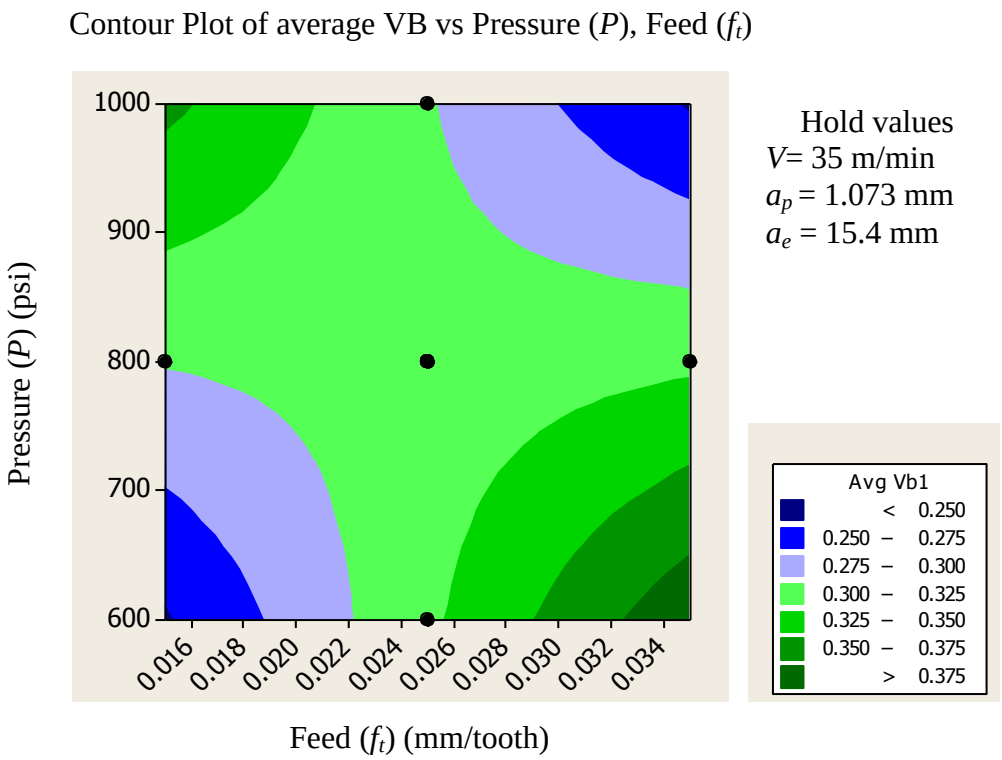

Figure 29: Contour plot (*P* vs. f_t)

Figure 29 shows the contour plot of Pressure (*P*) versus Feed (f_t), where curvature in the surface plot can be observed. At pressure value of 600 psi, as feed rate increases, the insert wear continues to increase. As the feed rate increases thicker chips are produced, hence cutting load increases. These increases in cutting load cause faster wear. Evidence of increase in insert wear with increase in feed rate can be found in the literature review. López, Pérez et al. 2000 have found have that as cutting load increases, tool wear increases. At 1000 psi, as feed rate increases, the insert wear rate reduces. One possible explanation is that with an increase in coolant pressure

directed through a nozzle at the cutting interface, the chip generated is smaller in size thus reducing the cutting load. This reduction in load reduces insert wear. This also explains the gradual decrease in insert wear when the feed rate is kept constant at 0.034 mm/tooth and the pressure is increased from 600 psi to 1000 psi. When the feed rate is kept constant at 0.016 mm/tooth and pressure is increased from 600 psi to 1000 psi, there is an increase in insert wear. One possible explanation for this anomaly could be the high value of speed corresponding to the low feed rate. Jawaid, Sharif et al. (2000) have found that for lower speeds, the tool wear is lower. It may also be argued that the extreme high pressure coolant may cause the coating on the insert to erode faster, exposing the bare un-coated metal. This could cause an accelerated tool wear at high pressure.

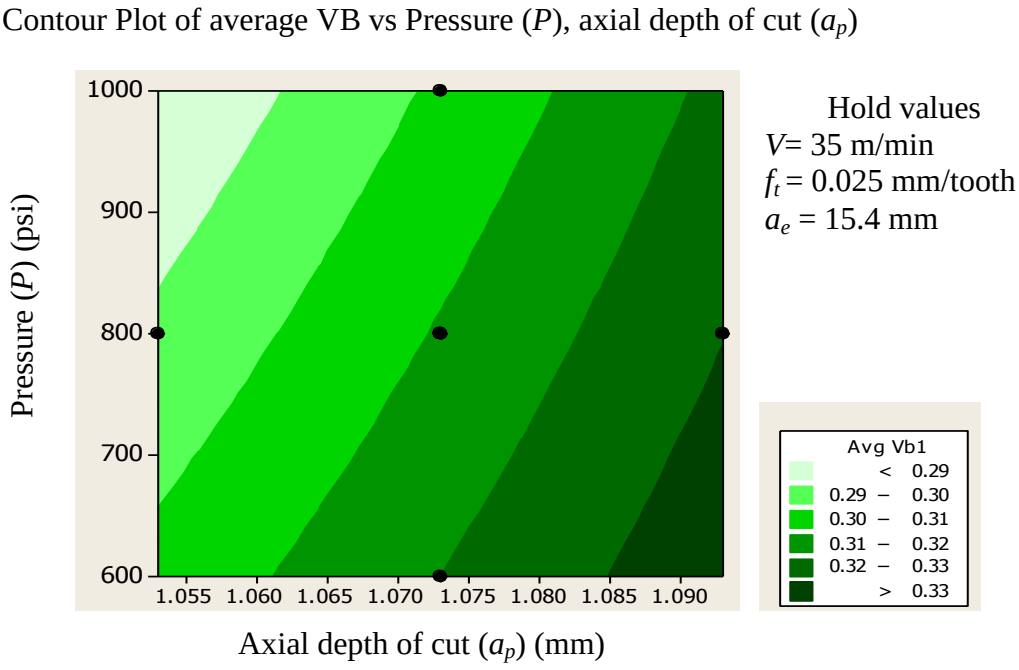

Figure 30: Contour plot (P vs. a_p)

Figure 30 shows the contour plot of Pressure (P) versus axial depth of cut (a_p). There is no sign of curvature in the plot. It can also be seen that the wear curves are not parallel to the Y axis.

When the axial depth of cut is kept constant, both at 1.055 mm and 1.090 mm and the pressure is increased from 600 psi to 1000 psi, the insert wear rate gradually decreases. This decrease is not significant and may be attributed to effective flushing of chips from the cutting zone due to high pressure. From the graph it is evident that pressure is not effectively able to delay the onset of wear when the contact length increases from 1.055 mm to 1.090 mm.

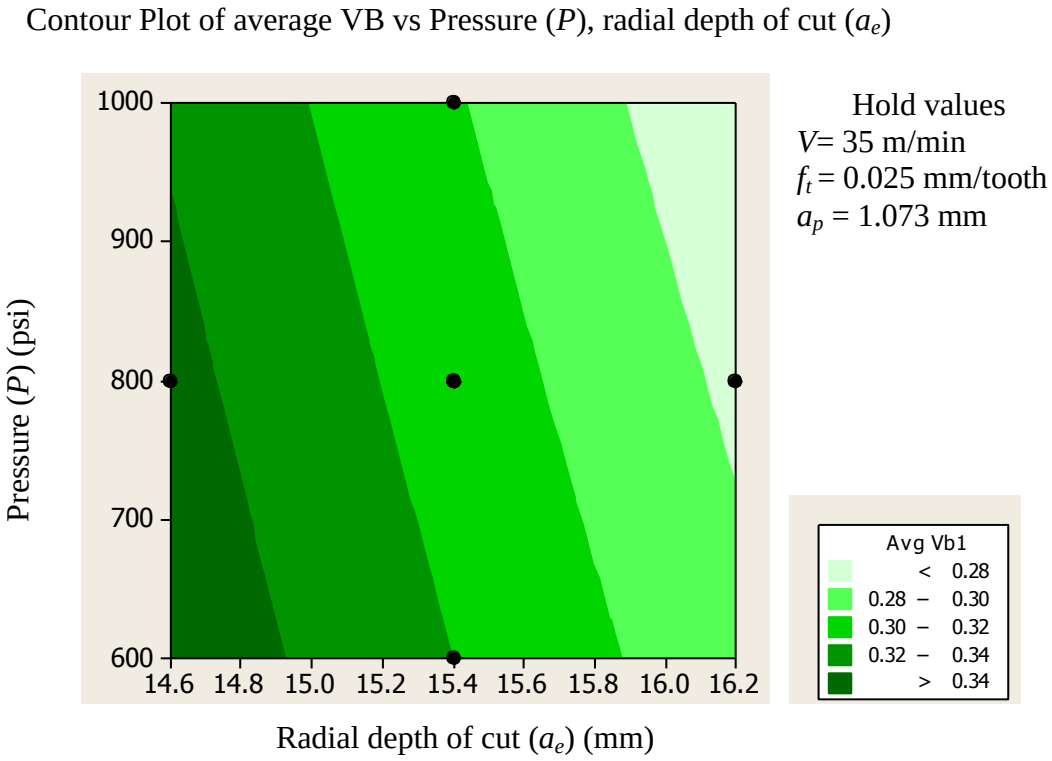

Figure 31: Contour plot (P vs. a_e)

Figure 31 shows the contour plot of Pressure (P) versus radial depth of cut (a_e). There is no sign of curvature in the plot. It can also be seen that the wear curves are not parallel to the Y axis. When the coolant pressure is kept constant, either at 600 psi or 1000 psi and the radial engagement of the tool is increased from 14.6 mm to 16.2 mm, it is seen that the insert wear gradually reduces. Physically however, as the radial engagement of the tool with the specimen is increased, it leads to thicker chips and increase in the temperature at the cutting interface. High

temperature so close to the tool is the principal reason for tool wear. However from the graph, it can be seen that even as the radial engagement increases, the insert wear decreases. Su, He et al. (2006) presents evidence of relation between tool wear and temperature. One possible explanation is that increase in pressure effectively breaks the thicker chips and conducts the heat away from the cutting zone, thereby delaying the insert wear. This same phenomenon explains the delay in insert wear when pressure is increased from 600 psi to 1000 psi.

5. CONCLUSION

There has been extensive research done in the field of machinability of titanium alloys and use of high pressure coolant in machining. However, until now, there was no work done to address the effect that high pressure coolant had in the milling of titanium alloy. This work has tried to address this gap in the literature. The experiment and analysis carried out in this research gives a brief yet insightful approach to the use of high pressure coolant in the milling of titanium alloys. The results from this experiment can recommend parameters of the cutting factors in order to obtain the minimal tool wear. Under similar cutting conditions, machining with a high factor setting of feed, radial depth of cut and pressure coupled with the low factor setting of speed and axial depth of cut, minimal tool wear condition may be obtained. The extensive analysis carried out with the model leads us to the following conclusions about the influence of pressure in this research. Within the parameter limits of this experiment:

- Pressure (P) was not found to be a significant main effect
- Pressure (P) and feed (f_t) were found to interact positively

Based on literature review and analysis from the experiments performed it can be inferred that:

- Pressure (P) may play an effective role in breaking the chips generated from machining, reducing the cutting load and thus preventing roughing of the tool
- Pressure (P) may play an effective role in conducting heat away from the cutting zone, thus reducing the thermal fatigue

6. FUTURE WORK

Future research work concentrating on tool wear while machining under high pressure coolant can focus on considering additional factors. All analysis and conclusions were based on the considered five factors in the experiment. More extensive analysis can be performed by considering factors like tool vibration during cutting, different coolant concentration, specimen hardness. To date, there has been no published research on interaction of high pressure coolant with the above mentioned factors.

Response surface methodology is a good tool to optimize the response in the direction of interest, but other algorithms like artificial neural network, fuzzy logic etc. can be used to do the same analysis. Direction of steepest descent was used to minimize the response i.e. average flank wear on the insert. More responses like material removal rate, cutting force etc. can be considered for analysis. More information about cutting forces on the insert and resulting stress can be collected and analyzed. Advanced metrology approach can be used to analyze the thermal stresses on the insert while machining. It can be argued that the extreme high pressure coolant may cause the coating on the insert to erode faster, exposing the bare un-coated metal. This theory could be tested by recording the coating thickness before and after machining. Specimen hardness can be measured before and after machining and differences, if any can be analyzed.

A validated mathematical model can be established from this experiment and this mathematical model can be used as a future work to simulate the factors involved in order to predict the wear rate. A more comprehensive approach can be used to consider a wider range of factor level combinations. Significant interactions can then be analyzed in greater detail.

7. REFERENCES

Arrazola P. J, A. Garay, Iriarte, L. M, Armendia, M, Marya, S, Le Maître, F. (2009). "Machinability of titanium alloys (Ti6Al4V and Ti555.3)." Journal of materials processing technology 209(5): 2223-2230.

Bajic, D., B. Lela, Zivkovic, D. (2008). "Modeling of machined surface roughness and optimization of cutting parameters in face milling" Metalurgija 47(4): 331-334.

Ezugwu, E. O., J. Bonney (2004). "Effect of high-pressure coolant supply when machining nickel-base, Inconel 718, alloy with coated carbide tools." Journal of materials processing technology 153-154: 1045-1050.

Ezugwu, E. O., J. Bonney, Da Silva, R. B, Machado, A. R, Ugwoha, E (2009). "High productivity rough turning of Ti-6Al-4V alloy, with flood and high-pressure cooling" Tribology transactions 52(3): 395 - 400.

Ezugwu, E. O., R. B. Da Silva, J. Bonney, R. B, Machado (2005). "Evaluation of the performance of CBN tools when turning Ti-6Al-4V alloy with high pressure coolant supplies" International journal of machine tools and manufacture 45(9): 1009-1014.

Ezugwu, E. O., Z. M. Wang (1997). "Titanium alloys and their machinability--a review" Journal of materials processing technology 68(3): 262-274.

Hong, H., A. T. Riga, Gahoon, J. M, Scott, C. G (1993). "Machinability of steels and titanium alloys under lubrication" Wear 162-164 (Part 1): 34-39.

Hong, S. Y., I. Markus, Jeong, Woo-cheo (2001). "New cooling approach and tool life improvement in cryogenic machining of titanium alloy Ti-6Al-4V" International journal of machine tools and manufacture 41(15): 2245-2260.

ISO (1989) International Standard ISO 8688-2. - Tool life testing in milling - Part 2: End milling.

Jawaid, A., Sharif, S., Koksal, S. (2000). "Evaluation of wear mechanisms of coated carbide tools when face milling titanium alloys" Journal of materials processing technology 99 (1 - 3): 266 - 274.

Kahles, J. F., M. Field, D. Eylon, F.H. Froes (1985). "Machining of titanium alloys." Journal of metals: 27-35.

Kitagawa, T., A. Kubo, Maekawa, K (1997). "Temperature and wear of cutting tools in high-speed machining of Inconel 718 and Ti---6Al---6V---2Sn" Wear 202(2): 142-148.

Komanduri, R., B. F. Von Turkovich (1981). "New observations on the mechanism of chip formation when machining titanium alloys" Wear 69(2): 179-188

López de lacalle, L. N., J. Pérez, Llorente, J. I, Sánchez, J. A (2000). "Advanced cutting conditions for the milling of aeronautical alloys" Journal of materials processing technology 100(1-3): 1-11

Nandy, A. K., M. C. Gowrishankar, Paul S. (2009). "Some studies on high-pressure cooling in turning of Ti-6Al-4V." International journal of machine tools and manufacture 49(2): 182-198.

Nouari, M., A. Ginting (2006) "Wear characteristics and performance of multi-layer CVD-coated alloyed carbide tool in dry end milling of titanium alloy." Surface and coatings technology 200(18-19): 5663-5676.

Su, Y., N. He, Li L, Li X. L (2006) "An experimental investigation of effects of cooling/lubrication conditions on tool wear in high-speed end milling of Ti-6Al-4V" Wear 261(7-8): 760-766.

Wang, Z. G., M. Rahman, Wong Y S. (2005). "Tool wear characteristics of binderless CBN tools used in high-speed milling of titanium alloys" Wear 258(5-6): 752-758.

Wertheim, R., J. Rotberg, Ber A. (1992). "Influence of high-pressure flushing through the rake face of the cutting tool" CIRP annals - Manufacturing technology 41(1): 101-106.

APPENDICIES

8. APPENDICES

A. Okuma Multus B300

Specifications:

Machine		
Size	Height (mm)	2600
	Floor Space (mm)	3750 x 2050
	Weight (kg)	9500
Live-Tool Spindle	Speed Range (rpm)	10000
	Max Torque, 5min/cont (N-m)	65.7/41.8
Main Spindle	Spindle Speed (min^{-1})	38 – 5000
Travels	X Axis (mm)	580
	Y Axis (mm)	160
	Z Axis (mm)	945
	W Axis (mm)	1000
	C Axis (mm)	360
	B Axis Indexing (mm)	-30 – 195
Capacity	Maximum machining diameter (mm)	450
Motor	Standard power, main motor (hp)	20/15

B. ChipBlaster JV10

Specifications:

Machine		
Tank Size	Volume (gal)	50
Coolant pressure	Pressure (psi)	Continuous up to 1500
Coolant volume	Volume (gpm)	Automatic variable 3 to 10 gpm
Input Power	Power	37 Amps, 240 VAC 19 Amps, 480 VAC

C. Hirox microscope

Specifications:

Machine		
Camera	Digital camera	High resolution CCD, capable of capturing 30 fps
Communications	Integrated	Integrated computer with LCD display
Calibration	Internal	Inter calibration scale, automatically readjusts with change of magnification
Magnification	Zoom lens	35 – 2500 x magnification
Travel	XY direction	85 mm travel range
Rotation	Rotary stage	XY rotary stage base
Illumination	Internal light source	Metal halide arc light, adjustable

D. Program code for CNC machining

The Machine code written for Okuma Multus B300 in G-M code language,

```
G00 W1500                    (Rapid of sub spindle)
G50 SB=10000
G20 HP=4
(TOOL - 12 OFFSET - 12)      [Tool definition set]
(SANDVIK 690)                [Program name]
MT=01201
M321
G20 HP=4
M110
G94 SB=1200 M241 M63 M9 BA=90. G52 TL=012012
M13
M08
G138
G17
M146
G0 C0                        (Edit for different sides of specimen C0-C90-C180-C270)
M147
G127 B90
G0 Z2
X-1.0 Y-1.25                 (Change y value to set radial depth)
```

```
Z1.35
G1 Z1.25 F50          (Set z value here for depth) (Change the value of F here to set speed)
X3. F10
G0 Z5
M12 M9
G126
G136
M146
M109
G0 X1200
G20 HP=4
TL=012000
M02                   (End of program)
```

E. Dimension Elite 3D printer

Specifications:

Machine		
Material	Model material	ABS - black
Building	Max build size (mm)	203 * 203 * 305
Deposition	Layer thickness (mm)	0.178 or 0.254
Compatibility	Workstation compatibility	Windows® XP / Windows Vista®
Requirements	Power supply	110-120VAC, 15 Amp dedicated circuit 220-240VAC, 7 Amp dedicated circuit

F. Regression Analysis – Factorial experiment

Regression Analysis: Avg VB1 versus Speed, Feed, ADOC, RDOC, Pressure

```
The regression equation is
Avg VB1 = - 1.91 + 0.0284 Speed + 7.43 Feed + 0.609 ADOC + 0.0097 RDOC
          + 0.000021 Pressure


Predictor       Coef    SE Coef      T      P
Constant     -1.9137     0.8572  -2.23  0.050
Speed        0.02839    0.01570   1.81  0.101
Feed           7.428      3.140   2.37  0.040
ADOC          0.6092     0.2093   2.91  0.016
RDOC         0.00969    0.03568   0.27  0.792
Pressure   0.0000211  0.0001962   0.11  0.917


S = 0.313994   R-Sq = 63.5%   R-Sq(adj) = 45.3%


Analysis of Variance

Source          DF       SS       MS     F      P
Regression       5  1.71736  0.34347  3.48  0.044
Residual Error  10  0.98592  0.09859
Total           15  2.70328


Source    DF   Seq SS
Speed      1  0.32234
Feed       1  0.55168
ADOC       1  0.83494
RDOC       1  0.00727
Pressure   1  0.00114
```

G. Regression Analysis – Central composite design

Response Surface Regression: Avg Vb1 versus S, F, A, R, P

Estimated Regression Coefficients for Avg Vb1

Term	Coef	SE Coef	T	P
Constant	5.705	50.358	0.113	0.911
S	0.963	0.984	0.979	0.344
F	127.187	205.654	0.618	0.546
A	5.035	45.499	0.111	0.913
R	-3.682	2.436	-1.512	0.153
P	0.003	0.010	0.337	0.741
S*F	0.700	1.721	0.407	0.690
S*A	-1.188	0.860	-1.380	0.189
S*R	0.025	0.022	1.148	0.270
S*P	-0.000	0.000	-1.046	0.313
F*A	-115.000	172.065	-0.668	0.515
F*R	-0.125	4.302	-0.029	0.977
F*P	-0.032	0.017	-1.845	0.086
A*R	2.594	2.151	1.206	0.248
A*P	0.000	0.009	0.058	0.954
R*P	-0.000	0.000	-0.029	0.977

S = 0.0344131 PRESS = 0.193709
R-Sq = 62.25% R-Sq(pred) = 0.00% R-Sq(adj) = 21.81%

Analysis of Variance for Avg Vb1

Source	DF	Seq SS	Adj SS	Adj MS	F	P
Regression	15	0.027342	0.027342	0.001823	1.54	0.213
Linear	5	0.015744	0.005997	0.001199	1.01	0.446
S	1	0.005340	0.001135	0.001135	0.96	0.344
F	1	0.000561	0.000453	0.000453	0.38	0.546
A	1	0.002128	0.000015	0.000015	0.01	0.913
R	1	0.007211	0.002706	0.002706	2.29	0.153
P	1	0.000504	0.000134	0.000134	0.11	0.741
Interaction	10	0.011598	0.011598	0.001160	0.98	0.501
S*F	1	0.000196	0.000196	0.000196	0.17	0.690
S*A	1	0.002256	0.002256	0.002256	1.91	0.189
S*R	1	0.001560	0.001560	0.001560	1.32	0.270
S*P	1	0.001296	0.001296	0.001296	1.09	0.313
F*A	1	0.000529	0.000529	0.000529	0.45	0.515
F*R	1	0.000001	0.000001	0.000001	0.00	0.977
F*P	1	0.004032	0.004032	0.004032	3.40	0.086
A*R	1	0.001722	0.001722	0.001722	1.45	0.248
A*P	1	0.000004	0.000004	0.000004	0.00	0.954
R*P	1	0.000001	0.000001	0.000001	0.00	0.977
Residual Error	14	0.016580	0.016580	0.001184		
Lack-of-Fit	11	0.016418	0.016418	0.001493	27.64	0.010
Pure Error	3	0.000162	0.000162	0.000054		
Total	29	0.043921				